Chinese Chemical Letters 36 (2025) 110533

Contents lists available at ScienceDirect

Chinese Chemical Letters

journal homepage: www.elsevier.com/locate/cclet

Recent advances of $CuSbS_2$ and $CuPbSbS_3$ as photocatalyst in the application of photocatalytic hydrogen evolution and degradation

Xinlong Zheng[a,b], Zhongyun Shao[a,b], Jiaxin Lin[a,c], Qizhi Gao[a], Zongxian Ma[a,d], Yiming Song[a], Zhen Chen[a,b], Xiaodong Shi[a], Jing Li[a], Weifeng Liu[d], Xinlong Tian[a,*], Yuhao Liu[a,*]

[a] School of Marine Science and Engineering, State Key Laboratory of Marine Resource Utilization in South China Sea, School of Physics and Optoelectronic Engineering, Hainan University, Haikou 570228, China
[b] School of Chemical Engineering and Technology, Hainan University, Haikou 570228, China
[c] School of Cyberspace Security (School of Cryptology), Hainan University, Haikou 570228, China
[d] Mechanical and Electrical Engineering College, Hainan University, Haikou 570228, China

ARTICLE INFO

Article history:
Received 7 June 2024
Revised 2 October 2024
Accepted 8 October 2024
Available online 10 October 2024

Keywords:
$CuSbS_2$
$CuPbSbS_3$
Photocatalysis
Hydrogen production
Degradation

ABSTRACT

The realization of high-efficiency photocatalysis is greatly meaningful to overcome the issues of current energy and environment, in which the core factor is the exploration of photocatalysts with promising semiconductor properties. The Cu-based metal sulfide photocatalysts of $CuSbS_2$ and its derivative of bournonite $CuPbSbS_3$ possess the features of earth-abundant elements, strong photostability, visible-light range bandgap, and high absorption coefficient, possessing great potential for the realization of efficient photocatalytic applications. Although the photocatalysts of $CuSbS_2$ and $CuPbSbS_3$ have been investigated in photocatalysis application of hydrogen production and degradation, the exploration process is still in the early-development stage. In this review, the design concept and semiconductor properties of $CuSbS_2$ and $CuPbSbS_3$ are firstly introduced. Subsequently, the photocatalytic applications of $CuSbS_2$ and $CuPbSbS_3$ photocatalysts, mainly including hydrogen production and degradation, are systematically reviewed. Finally, the challenges and prospects for the further exploration of $CuSbS_2$ and $CuPbSbS_3$ photocatalysts are provided.

© 2025 Published by Elsevier B.V. on behalf of Chinese Chemical Society and Institute of Materia Medica, Chinese Academy of Medical Sciences.

1. Introduction

In the past decades, the continues consumption of traditional fossil energy sources makes it urgent to develop advanced renewable techniques for the acquirement of sustainable sources [1-15]. As one of the solar energy conversion technique, photocatalysis, is an ideal technique to solve the current development issues, in which the key factor is the efficient application of solar energy and exploration of photocatalyst with promising semiconductor properties [16-30]. In 1972, Fujishima *et al.* proved that the photoelectrochemical water splitting can be performed at the TiO_2 electrode [31], which pioneered the photocatalysis technique by the semiconductor photocatalyst of TiO_2. On this basis, great efforts have been made to optimize the photocatalytic performance of TiO_2 photocatalyst [32-36]. In addition, various kinds of metal oxide (MO) photocatalysts, typically ZnO, Bi_2O_3, CeO_2, WO_3, $SrTiO_3$, and $BiVO_4$, have also been explored and applicated in photocatalysis [37-42]. Nevertheless, owing to the O 2p state localized nature, the charge separation efficiency in MO photocatalysts is generally weak due to the heavy effective mass of the photogenerated holes [43]. Furthermore, most of the explored MO photocatalysts have wide bandgap due to the deep O 2p orbital of the valence band (VB) [44]. As a result, the photocatalytic application based on MO photocatalysts can be only performed under UV light irradiation, which accounts only ~4% of the sunlight. Therefore, for the realization of efficient visible-light photocatalytic process, the narrow bandgap semiconductor photocatalysts need to be explored.

Over the past decades in the research of photocatalysis, metal sulfide (MS) photocatalysts have been gradually explored in visible-light photocatalysis due to the general narrow bandgap (stem from the small effective mass and robust quantum size effect) along with other promising semiconductor features [45-49]. As shown in Fig. 1, compared with TiO_2 and other conventional metal oxide (MO) photocatalysts, the MS photocatalysts not only possess general narrow bandgap due to the robust quantum size effect and small effective mass, but have the negative conduction

* Corresponding authors.
E-mail addresses: tianxl@hainanu.edu.cn (X. Tian), yhliu@hainanu.edu.cn (Y. Liu).

https://doi.org/10.1016/j.cclet.2024.110533
1001-8417/© 2025 Published by Elsevier B.V. on behalf of Chinese Chemical Society and Institute of Materia Medica, Chinese Academy of Medical Sciences.

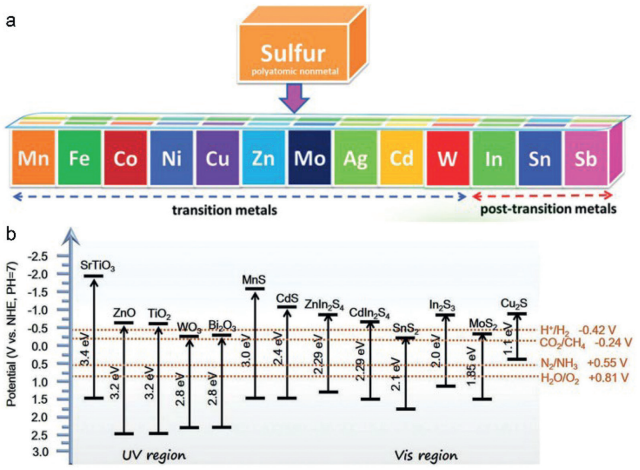

Fig. 1. (a) Representative transition metal sulfides and post-transition metal sulfides. Copied with permission [26]. Copyright 2019, Royal Society of Chemistry. (b) Energy band potentials of several representative MO and MS photocatalysts. Copied with permission [45]. Copyright 2022, Wiley Publishing Group.

band (CB) potential, which can provide strong hydrogen evolution reaction (HER) driving forces [50-53]. In addition, the MS photocatalysts with nanostructures generally exhibit large specific capacities, long carriers' lifetime, and high photosensitivity than the MO [54]. Owing to the high theoretical volume expansion, several representative MS photocatalysts own the layer structure, which is beneficial for the alleviate strain through volume expansion [55]. At the working temperature lower than the MO, the MS photocatalysts generally own higher sensitivity and selectivity to the specific classes of molecules [45]. Another unique feature of MS photocatalysts is the lower melting point, which is significantly different from the conventional MO photocatalysts [56]. In this case, the researches in the PHE application, focusing on the MS photocatalyst, is a meaningful scientific route for the realization of efficient PHE performance. Typically, the binary MS (BMS) photocatalysts have been firstly explored and researched due to the simple phase and fabrication process, representatively MoS_2, CdS, and CuS [52,57-62]. Although remarkable research progress has been made, some intrinsic issues of BMS photocatalysts still exist, which greatly hinder the further enhancement of the photocatalytic performance. Typically, Zheng *et al.* comprehensively summarized the research status of BMS photocatalysts in photocatalytic hydrogen evolution (PHE) and photocatalytic degradation (PD) applications [63]. The authors not only highlighted the advantages and semiconductor properties of the BMS photocatalysts, but pointed out the issues and drawbacks, including the photocorrosion phenomenon of CdS and stacked layers (or irregular aggregates) of MoS_2. The representative intrinsic drawbacks of other BMS photocatalysts were also pointed out. Therefore, for the further enhancement of photocatalytic performance, it is greatly significant to explore other kinds of MS photocatalysts, aiming to solve the above-mentioned issues of the BMS photocatalysts.

Compared with the early-developed BMS photocatalysts, the recently explored multinary MS (MMS) photocatalysts can effectively solved the drawbacks of BMS due to the features of flexible elements components, tunable bandgap and band structures, and promising photostability [54]. Especially, through the modification of phase transition or alloying, the band structures of the MMS photocatalysts are easy to be modulated, which is greatly beneficial to optimize the photocatalytic performance. In this regard, our group has systematically summarized the research progresses of the Ag, Cu, Zn-based MMS photocatalysts in photocatalytic applications, including $ZnIn_2S_4$, $CuInS_2$, $AgBiS_2$, $AgGaS_2$, $AgIn_5S_8$, and $AgInS_2$, especially in the photocatalytic application of PHE [64-67]. Although some drawbacks of BMS can be overcome by the MMS photocatalysts and promising research progress has been achieved, most of them need to be synthesized under expensive condition owing to the existence of earth-unabundant elements of Ga, Ag, Bi, and In. Hence, an efficient strategy to decrease the fabrication cost of MMS photocatalyst can further broad the MMS photocatalysts in photocatalytic applications.

Taking the $CuInS_2$ as the prototype, the low-cost MMS photocatalyst of $CuSbS_2$ can be formed through replace the In element in $CuInS_2$ by the Sb, which is the periodical production and groundbreaking research progress of the MMS photocatalysts [68-71]. At the same time, many other types of photocatalyst materials have been widely explored, especially the MOs and perovskite-structured compounds [72-75]. Nevertheless, the photo-stable MOs can only absorb the UV-light due to the wide bandgap, and perovskite-structured photocatalysts generally suffer from the low stability due to the high sensitivity to water and oxygen. Therefore, the $CuSbS_2$ photocatalyst can not only overcome the drawbacks of these photocatalysts for contemporaneous research but is potential to realize efficient PHE under low-cost condition, which is highly valuable for the exploration in the PHE field. Recently, the photocatalysts of $CuSbS_2$ and $CuSbS_2$-based heterojunction photocatalysts of $CuSbS_2/TiO_2$ have been successfully applicated in PHE and PD applications [64]. Moreover, based on the advanced concept of "electronic dimensionality", the $CuSbS_2$ can be reconstructed to the MMS photocatalyst of bournonite $CuPbSbS_3$ after the incorporation of PbS, which is greatly beneficial in solar-to-energy (STE) applications due to the excellent semiconductor properties of 3D electronic dimensionality, visible-light bandgap of 1.3 eV, and defect-tolerant [76]. In the initial exploration stage, the $CuSbS_2$ and $CuPbSbS_3$ were mainly applicated in the STE application of thin-film solar cell and achieved phased research progress [76-81]. Guided by the research experience of Ag, Cu, Zn-based MMS photocatalysts and appropriate semiconductor properties of $CuSbS_2$ and $CuPbSbS_3$, great research efforts have been made to take them in the application of photocatalysis since 2020 (the first photocatalytic application report of $CuSbS_2$ in PHE [82]).

In parallel with the increasing researches on MS photocatalysts, along with the arising of $CuSbS_2$ and $CuPbSbS_3$, several reviews have focused on the photocatalytic applications. Typically, Zhu *et al.* summarized the MS photocatalysts developed over the past decade in the application of PHE, carbon dioxide reduction, nitrogen reduction, and PD on the pollutant removal, including CdS, SnS_2, Cu_2S, and $ZnIn_2S_4$ [45]. Moreover, the recently highly concerned MS photocatalysts of $ZnIn_2S_4$ has also been summarized by several groups, focusing on comprehensive photocatalytic applications [66,83-87]. Despite impressive achievements have been realized on these MS photocatalysts, a timely review focusing not only the on the researching meaning of recently emerged $CuSbS_2$ and $CuPbSbS_3$ but on the corresponding photocatalytic applications is missing. In this review, a timely review of $CuSbS_2$ and $CuPbSbS_3$ photocatalysts in photocatalytic application is proposed. Specifically, the basic semiconductor properties of $CuSbS_2$ and $CuPbSbS_3$ are firstly introduced. Subsequently, the recent research progresses of $CuSbS_2$ and $CuPbSbS_3$ in photocatalytic applications, including PHE and PD, are summarized and discussed. Finally, the current issues and future research routes of $CuSbS_2$ and $CuPbSbS_3$ in photocatalytic applications are presented.

2. Basic semiconductor properties of $CuSbS_2$ and $CuPbSbS_3$

2.1. Crystal structures

In the crystal structure of $CuSbS_2$, the twisted Cu–S pentahedra and Sb–S tetrahedra are mainly comprised, forming the 2D layer

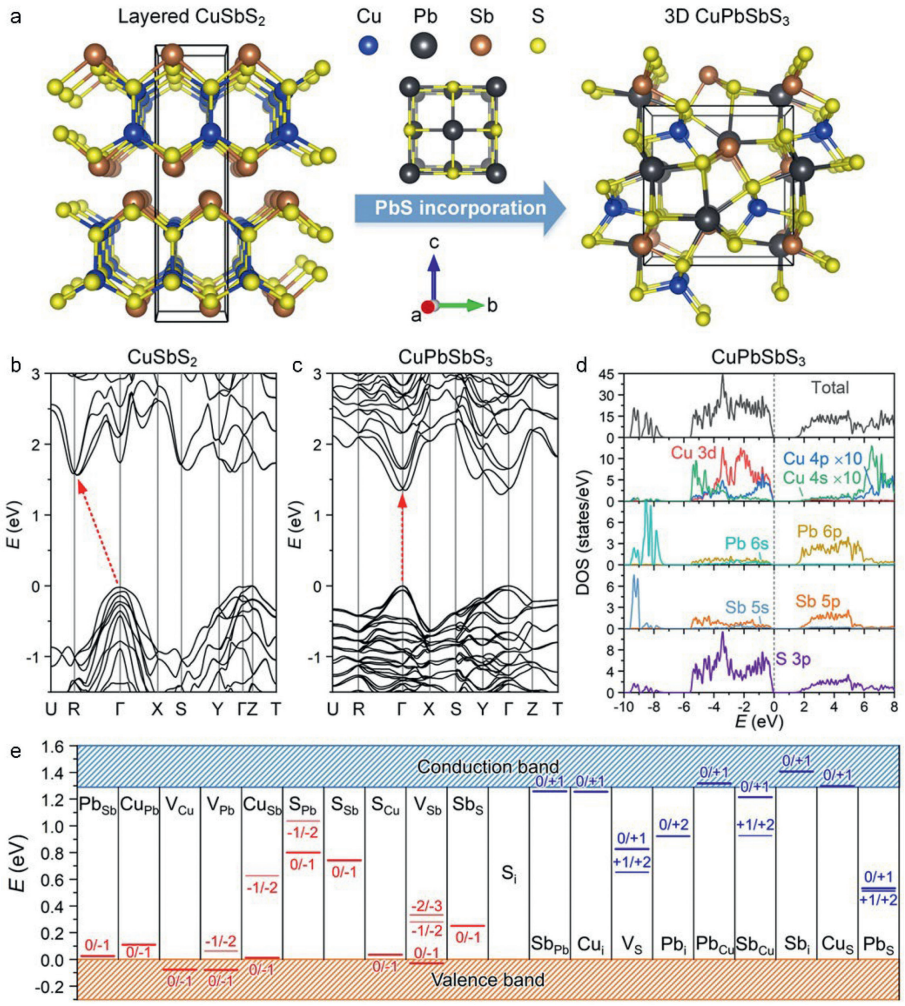

Fig. 2. (a) Crystal structure of $CuSbS_2$ and the reconstructed of $CuPbSbS_3$ after the incorporation of PbS. Band structures of (b) $CuSbS_2$ and (c) $CuPbSbS_3$. (d) Calculated density of states and (e) intrinsic defects charge-state transition levels of $CuPbSbS_3$. Copied with permission [76]. Copyright 2020, Elsevier.

crystal structure and orthorhombic system. The ordered cations of Cu and Sb are intermixed through the ternary compound with an ideal lattice (left part of Fig. 2a). Moreover, in each unit cell of $CuSbS_2$, the atom amounts of Cu, Sb, and S are 4, 4, and 8, respectively (the cube in the left part of Fig. 2a), in which the coordinated number of Cu and Sb surrounding the S atoms are 3 and 4 [70]. During the STE process, the electron clouds overlap in each crystal layers can be prevented due to the feature of 2D monolayered crystal structure, which allows efficient charge transfer in the intra-layer manner. On the other hand, the obvious disadvantage of this structure is the blocking charge transfer along the out-of-plane direction and low density of specific surface area [88]. Guided by the concept of electronic dimensionality proposed by Xiao *et al.*, the promising semiconductor materials for the realization of efficient STE is high electronic dimensionality (3D electronic dimensionality), in which the precondition is the 3D crystal structure [89]. Specifically, the electronic dimensionality is intrinsically defined as the orbitals connectivity, which comprises the CB minimum and VB maximum [89]. In this case, the bandgap, isotropy, and thus electronic properties are strongly affected by the electronic dimensionality. Up to now, several researches have experimentally and theoretically proved that the high electronic dimensionality (3D electronic dimensionality) provides the potential for high STE performance [76,90-92]. Typically, the mainstream semiconductor materials in the STE application of photovoltaics are not only crystallographically 3D but electronically 3D, like Si, CdTe, GaAs, and Cu(In,Ga)Se_2, and perovskite of $CH_3NH_3PbI_3$ [93-96]. Hence, the concept of electronic dimensionality commendably accounts for the predicting and understanding of the optoelectronic properties of semiconductor materials. Aiming to stable the filled lone-pair s^2 states, $CuSbS_2$ tends to crystallize into 2D crystal structures due to the structural distortion. Although promising research progresses of $CuSbS_2$ in STE application have been achieved, especially in thin-film solar cell, the corresponding STE efficiency is still lower than the mainstream semiconductor materials, resulting in the further exploration of advanced semiconductor materials with electronically 3D. During the exploration process of perovskite, especially the $NH_3CH_3PbI_3$, various studies have proved that the heavy post-transition metal of Pb possesses the feature of less active lone pair states [95,97-106]. Therefore, the MS semiconductor materials, containing the Pb element, can easily crystallize to the crystal structure of 3D rocksalt-type along with 6 coordination number [88]. As expected, the layer crystal structure of $CuSbS_2$ can reconstructed to the 3D crystal structure of $CuPbSbS_3$ after the incorporation of PbS (right part of Fig. 2a) [76].

2.2. Band structures

Theoretically, the bandgap of $CuSbS_2$ is calculated to be 1.56 eV of indirect (Fig. 2b), which is basic in agreement with the experimental values [107]. Therefore, although the $CuSbS_2$ can effectively solved the high-cost issue of $CuInS_2$, the intrinsic indirect bandgap

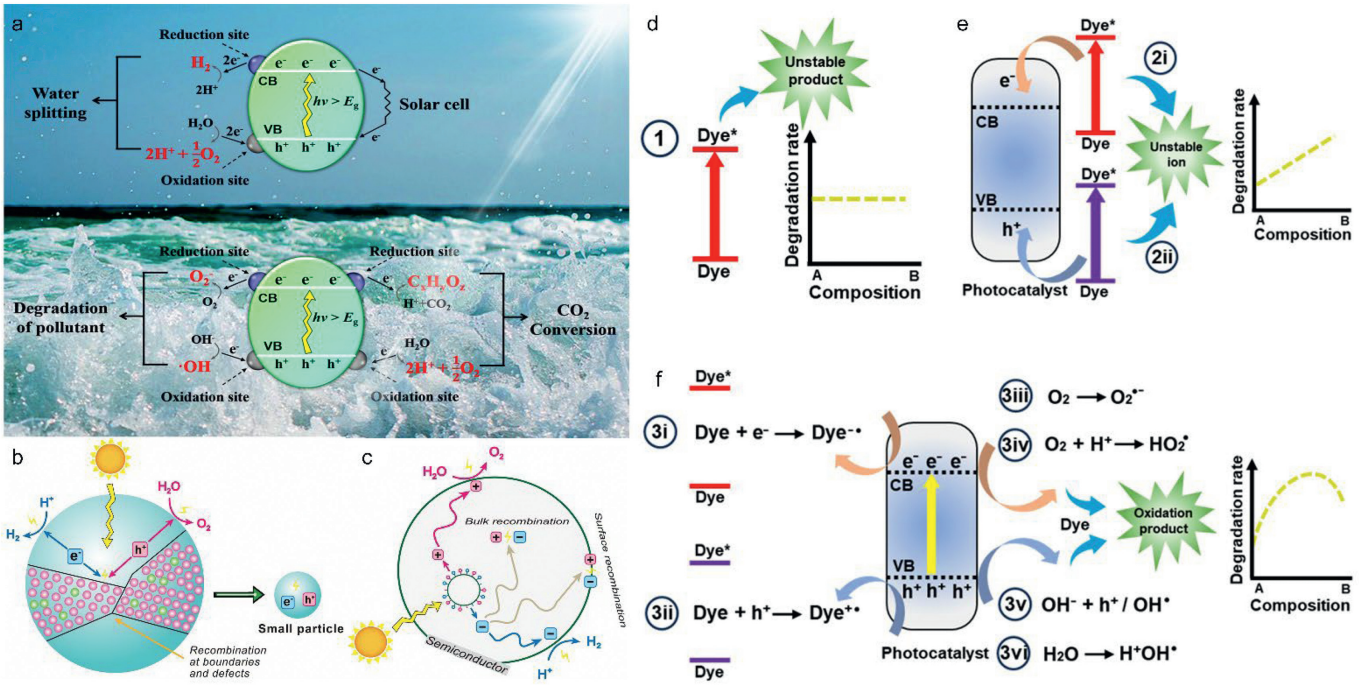

Fig. 3. (a) Basic mechanisms of PHE and PD. Reproduced with permission [109]. Copyright 2020, Elsevier. (b) Charge migration and (c) bulk and surface recombination behaviors during the PHE process. Copied with permission [54]. Copyright 2024, Wiley Publishing Group. The development process of PD process: (d) conventional degradation, (e) direct degradation, and (f) PD through photogenerated carriers' injection. Reproduced with permission [110]. Copyright 2017, Springer Nature.

is not ideal for high-efficiency STE. For $CuPbSbS_3$, the corresponding bandgap is theoretical 1.29 eV by including the spin−orbit coupling to eliminate the overestimation (Fig. 2c). Furthermore, the experimental bandgap is also an essential factor to evaluate the photocatalytic application potential of $CuSbS_2$ and $CuPbSbS_3$ photocatalyst. Experimentally, the bandgap of the semiconductor photocatalyst is generally estimated by the UV–vis spectrum, in which the linear increase of light absorption with increasing energy is the characteristic of semiconductor photocatalyst [108]. According to the equation of $E_g = 1240/\lambda_g$, in which the E_g is the value of bandgap and λ_g is the optical absorption edge, the E_g of the direct bandgap semiconductor can be basically estimated. Aiming to achieve more accurate calculation, the Tauc plot equation of $(\alpha h\nu)^{1/n} = A(h\nu - E_g)$ (n = 1/2 for direct; n = 2 for indirect) can be used to verify the E_g of both direct and indirect bandgap semiconductors [108]. For valence band (VB) of $CuPbSbS_3$, it mainly composes of the orbitals of Cu 3d/Pb 6s/Sb 5s and S 3p with antibonding states, whereas the CB is Cu 4s/Pb 6p/Sb 6p and S 3p orbitals (Fig. 2d). As a result, the $CuPbSbS_3$ possesses 3D electronic dimensionality due to the reason that the VB and CB are contributed by all atoms in it [76]. Therefore, $CuPbSbS_3$ is expected to exhibit good charge transfer properties due to the dispersive band edges caused by the 3D electronic dimensionality. The theoretical point defects charge-state transition levels of $CuPbSbS_3$ are shown in Fig. 2e. Obviously, the six dominant defects of V_{Cu}, Cu_i, V_{Pb}, Cu_{Pb}, Pb_{Sb}, and Sb_{Pb} have lower ΔH_f values, whereas the defects of V_S, S_{Pb}, V_{Sb} etc. have high ΔH_f values with deep states. Hence, in the bandgap of $CuPbSbS_3$, the deep states are absence and all the dominant defects are shallow defects, indicating the defect-tolerant feature of $CuPbSbS_3$.

3. Basic mechanisms of PHE and PD

The basic mechanisms of PHE and PD are inductively illustrated in Fig. 3a [109]. Holistically, the photocatalytic procedure mainly includes three process: (i) Photogenerated carriers, including electrons and holes, are formed after light irradiation on the semiconductor photocatalyst; (ii) Part of the photogenerated electrons and holes are recombined and others are migrated to the photocatalyst surface; (iii) Photogenerated electrons and holes on the surface of the photocatalyst directly participate in reduction and oxidation reactions, respectively. During the whole photocatalytic process, there are several key points need to be considered. Firstly, photogenerated electron−hole pairs are formed after the electrons on the semiconductor VB transfer to the CB. Secondly, the CB or VB potentials of the semiconductor photocatalyst need to locate at the appropriate position, making it suitable for the corresponding photocatalytic applications. Specifically, for the semiconductor photocatalyst, the CB potential should be more negative than the potential of hydrogen production (0 eV) or thermodynamic superoxide radical generation (−0.046 eV) (*vs.* NHE, pH 0). Similarly, the VB potential should be more positive than the oxidation position of the organics, like the dye, Rhodamine B (RhB), and antibiotics. Moreover, the $^{\bullet}OH$ radicals, an important role during the PD process, are generally originated from two aspects of multistep reduction by photoelectrons and oxidization of water (OH^-) by photogenerated holes. Statistically, for the realization of efficient PD of the semiconductor photocatalyst, the corresponding VB potential should be more positive than 2.38 eV (*vs.* NHE, pH 0), which involves the thermodynamic demand.

During the PHE process, the charges migration process is generally along with the bulk and surface recombination, which is affected by the intrinsic properties of the semiconductor photocatalyst, typically crystallinity, micro size, crystal structure, and active sites (Figs. 3b and c). The final PHE performance of the semiconductor photocatalysts greatly depend on the HER-participating photogenerated electrons density, in which the precondition is the effective hinderance of the charge recombination [66]. Therefore, all effective optimization strategies should be taken to maximize the density of HER-participating photogenerated electrons. For the MS photocatalysts, the access to HER exploitation is easily allowed due to the favorable energy band and capacity of light-harvesting.

On the contrary, owing to the tendency for oxidizing the lattice S ions of photogenerated holes (rather than water or oxygen splitting), the corresponding oxygen evolution reaction process of MS photocatalysts is difficult to realize. In this case, several electron donors (sacrificial reagent) are generally introduced to consume the photogenerated holes to boost the HER, typically Na_2S/Na_2SO_3, lactic acid, and triethanolamine [54]. For the PD process, the introduction of photocatalysts in the conventional degradation process can greatly accelerate the degradation process (Figs. 3d and e) [110]. Specifically, compared with the conventional degradation process in the absence of photocatalyst, the electrons in the semiconductor photocatalysts can be injected by the excited dye under the light irradiation, forming the oxidized radial cation of $Dye^{+\bullet}$ (2i in Fig. 3e). At the same time, the process of photocathodic sensitization can form the reduced radical dye ($Dye^{-\bullet}$) (2ii in Fig. 3e). The final PD performance greatly depends on the chemical force between the redox potential and degradation photocatalyst of the dye. As shown in 3i and 3ii in Fig. 3f, the radical intermediate species can be generated by the chemical reaction of photogenerated electrons and holes, in which the dyes (organics) can be effectively degraded (3iii–3vi in Fig. 3f). In this process, the degraded organic component, mainly including H^+, OH^-, and H_2O, are absorbed on the surface of the photocatalyst, and the final degradation rate is mainly determined by the corresponding absorption density. Among the chemical reaction of 3i−3vi, the enhancement of charge life time or carriers' density in one of the parts can also effectively enhance the PD rate, which is similar to the optimization route of PHE. Therefore, for the realization of efficient PHE or PD, the selection of the semiconductor photocatalyst is an important precondition, which highlights the material evolution of $CuSbS_2$ and $CuPbSbS_3$.

4. PHE and PD applications of $CuSbS_2$ and $CuPbSbS_3$

4.1. $CuSbS_2$

4.1.1. Initial application of $CuSbS_2$ photocatalyst in photocatalysis

In 2020, Sarilmaz *et al*. synthesized the $CuSbS_2$ photocatalyst with different shapes through a facile hot-injection method and applicated in PHE [82], which pioneered the STE application of $CuSbS_2$ in photocatalysis. Specifically, the morphology of synthesized $CuSbS_2$ photocatalyst, characterized by the scanning electron microscopy (SEM) and elemental dispersive X-ray (EDX) analysis, has two shapes of rod (R-$CuSbS_2$) and dot (D-$CuSbS_2$) (Figs. 4a and b) and the structural shapes effects of them on PHE performance are investigated. The results showed that the hydrogen production rate of $CuSbS_2$ photocatalyst was effectively promoted by tuning the corresponding shapes due to the optimized CB potentials of R-$CuSbS_2$ or D-$CuSbS_2$, which are more negative than the hydrogen production potential (Fig. 4c). Moreover, the corresponding PHE rates were measured to be R-$CuSbS_2$ > D-$CuSbS_2$ owing to the more efficient charge separation of 1D microrod catalysts. Therefore, this work not only pioneered the $CuSbS_2$ in the application of photocatalysis but provide an efficient path to optimize the corresponding physicochemical property.

4.1.2. $CuSbS_2$-based photocatalysts with further optimization

In addition to the shape tuning method mentioned above, other optimization strategies of semiconductor photocatalyst have also been established. Guided by the deeper explored MS photocatalysts, like CdS, MoS_2, $AgIn_5S_8$, $CuInS_2$, $ZnIn_2S_4$, and Cu_2ZnSnS_4 (CZTS), the corresponding optimization strategies mainly include the controlling of morphology and structure, doping by the trace element (less than 1%), introduction of vacancies (a certain amount of point defects), Schottky junction formation through cocatalyst loading (generally noble-metal cocatalyst), and heterojunction construction [66,111]. Among these optimization strategies, the heterojunction construction, composed of two or more than two semiconductor photocatalysts, has been proved to be the most effective path due to the enhanced charge separation efficiency in the interface [54,112-115]. Guided by this, researchers have also attempted to improve the photocatalytic activity of $CuSbS_2$ photocatalyst through the construction of $CuSbS_2$-based heterojunction. Typically, Wang *et al*. recently designed an efficient strategy by adjusting the band alignment to enhance the photocatalytic activity of $CuSbS_2$ photocatalyst, specifically in both PHE and PD [116]. The authors synthesized the $CuSbS_2$-based heterojunction photocatalyst of $CuSbS_2$/CdS/ZnO through a three-step irradiation process by the microwave (Fig. 4d), aiming to demonstrate the energy band structure influence on photocatalytic activity. On the basis of the heterojunction construction of $CuSbS_2$/ZnO, the introduction of CdS can further regulate the band alignment to translate the "cliff-like" CB of $CuSbS_2$/ZnO to the "spike-like" (Fig. 4e), which greatly hinders the charge recombination and realizes a full degradation of RhB after 80 min under the simulation solar light. Moreover, the change of the charge transfer mechanism transformation can raise the photogenerated electrons energy level, making the $CuSbS_2$/CdS/ZnO with a certain PHE capacity of 42.37 μmol g^{-1} h^{-1}. Therefore, this work not only realized a deeper exploration of $CuSbS_2$ photocatalyst through the heterojunction construction but broaden the corresponding photocatalytic application from PHE to PD.

In consideration of the early-exploration of $CuSbS_2$ in photocatalytic application and positive effects of heterojunction construction, the heterojunction photocatalysts based on $CuSbS_2$ in the application of photocatalytic, especially in the RhB degradation, have also been reported. Representatively, Zhi *et al*. constructed the Z-scheme heterojunction photocatalyst of $CuSbS_2$/ZnO by a two-step microwave irradiation method, in which the ZnO nanosheets are compounded with $CuSbS_2$ tetragonal particles aggregate. In this heterojunction structure, the light absorption efficient and specific surface area can be both optimized by tuning the ZnO concentration [117]. In the PD process, the degradation efficiency of RhB reached 100% after 120 min due to the low charge transfer impedance, high absorbency, and hindered charge recombination. Combining the theoretical calculation and experimental characterization, the authors have demonstrated that the photogenerated electrons can only participate the HER at a lower CB than the $O_2/O_2^{-\bullet}$ couple potential (CB of $CuSbS_2$) and photogenerated holes at higher VB than the $H_2O/HO^\bullet$ couples potential (VB of ZnO) (Fig. 4f). Therefore, this work provided a $CuSbS_2$-based Z-scheme heterojunction photocatalyst for the organic pollution treatment strategy. Similarly, the authors have also attempted to construct the type-II heterojunction photocatalyst of $CuSbS_2/TiO_2$ and realized a preliminary degradation of RhB (Fig. 4g) [118].

4.1.3. Summary of $CuSbS_2$ in photocatalytic applications

Combining with the corresponding research progress, it is obvious that the semiconductor photocatalyst of $CuSbS_2$ has realized the lower synthesis cost of MMS photocatalysts almost without any loss of the photocatalytic performance. Nevertheless, the indirect bandgap and layer structure of $CuSbS_2$ leads to the blocking of active sites and relative low charge transfer efficiency, which is harmful for the realization of high-efficiency photocatalytic performance to some extent. Although the issues can be overcome by the controlling of morphology and construction of heterojunction, which have been realized by the above-mentioned works, the inherent drawbacks of $CuSbS_2$ still limits the further groundbreaking progresses in the photocatalysis field. Thus, more advanced MMS photocatalyst based on the $CuSbS_2$ prototype is rising to be explored, aiming to further promote the photocatalytic application.

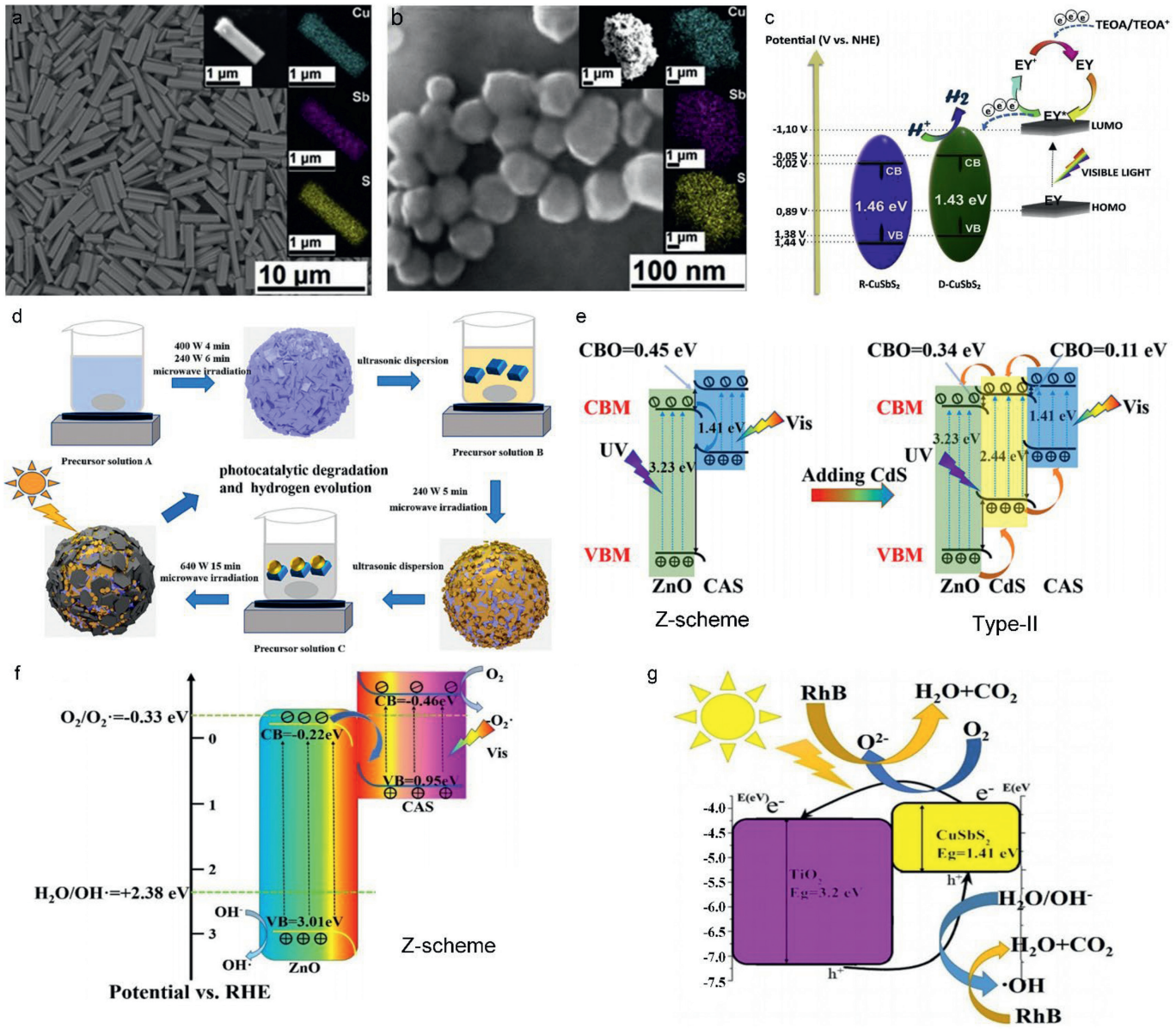

Fig. 4. (a) SEM and (b) EDX images of R-$CuSbS_2$ and D-$CuSbS_2$. (c) Proposed PHE mechanism of $CuSbS_2$ photocatalyst with different shapes. Copied with permission [82]. Copyright 2020, Elsevier. (d) Synthesis process and (e) band structure and charge migration mechanism of $CuSbS_2$/CdS/ZnO heterojunction photocatalyst. Copied with permission [116]. Copyright 2023, Elsever. Proposed mechanism of $CuSbS_2$-based heterojunction photocatalyst in PD of RhB: (f) $CuSbS_2$/ZnO and (g) $CuSbS_2$/TiO_2. Copied with permission [117]. Copyright 2022, Wiley Publishing Group. Copied with permission [118]. Copyright 2020, Springer.

4.2. $CuPbSbS_3$

4.2.1. Exploration of $CuPbSbS_3$ in STE applications

After the incorporation of PbS, the $CuSbS_2$ with layer crystal structure and indirect bandgap can be restored to the bournonite $CuPbSbS_3$ with 3D crystal structure and direct bandgap, which possesses better semiconductor properties to realize higher photocatalytic performance. Innovatively, Frumar *et al.* (1973) firstly explored the crystal structure and powder fabrication of $CuPbSbS_3$ [119], which highlighted the STE application of it. Until recent years, researchers have attempted to take the $CuPbSbS_3$ in the application of thin-film photovoltaics by the combination of theoretical and experimental studies and achieved promising progress [76,120-123]. As one of the deeper-explored Cu-based MMS semiconductor material, the CZTS have also been widely studied in the field of thin-film photovoltaics, aiming to decrease the fabrication cost of $Cu(In,Ga)(S,Se)_2$ [93,124-132]. With the deepening of the studies, researchers found that the CZTS is not only suitable for the application of thin-film photovoltaics but also for photocatalysis due to the appropriate semiconductor properties, like 1.5 eV direct bandgap, sparse band structure, and high absorption coefficient [133]. As expected, CZTS-based photocatalysts have realized promising progresses in photocatalytic applications of PHE, PD, and photoelectrocatalysis [134-141]. In view of the excellent semiconductor properties of $CuPbSbS_3$ and the application expansion of CZTS from thin-film photovoltaics to photocatalysis, the $CuPbSbS_3$ semiconductor materials also holds great potential to achieve efficient photocatalytic applications, in which the key factor is the fabrication of $CuPbSbS_3$ photocatalyst.

4.2.2. Initial application of $CuPbSbS_3$ photocatalyst in photocatalysis

In 2022, our group synthesized the $CuPbSbS_3$ photocatalyst with the morphology of nanoflakes through a facile butyldithiocarbamate acid (BDCA) solution process [142], in which the BDCA

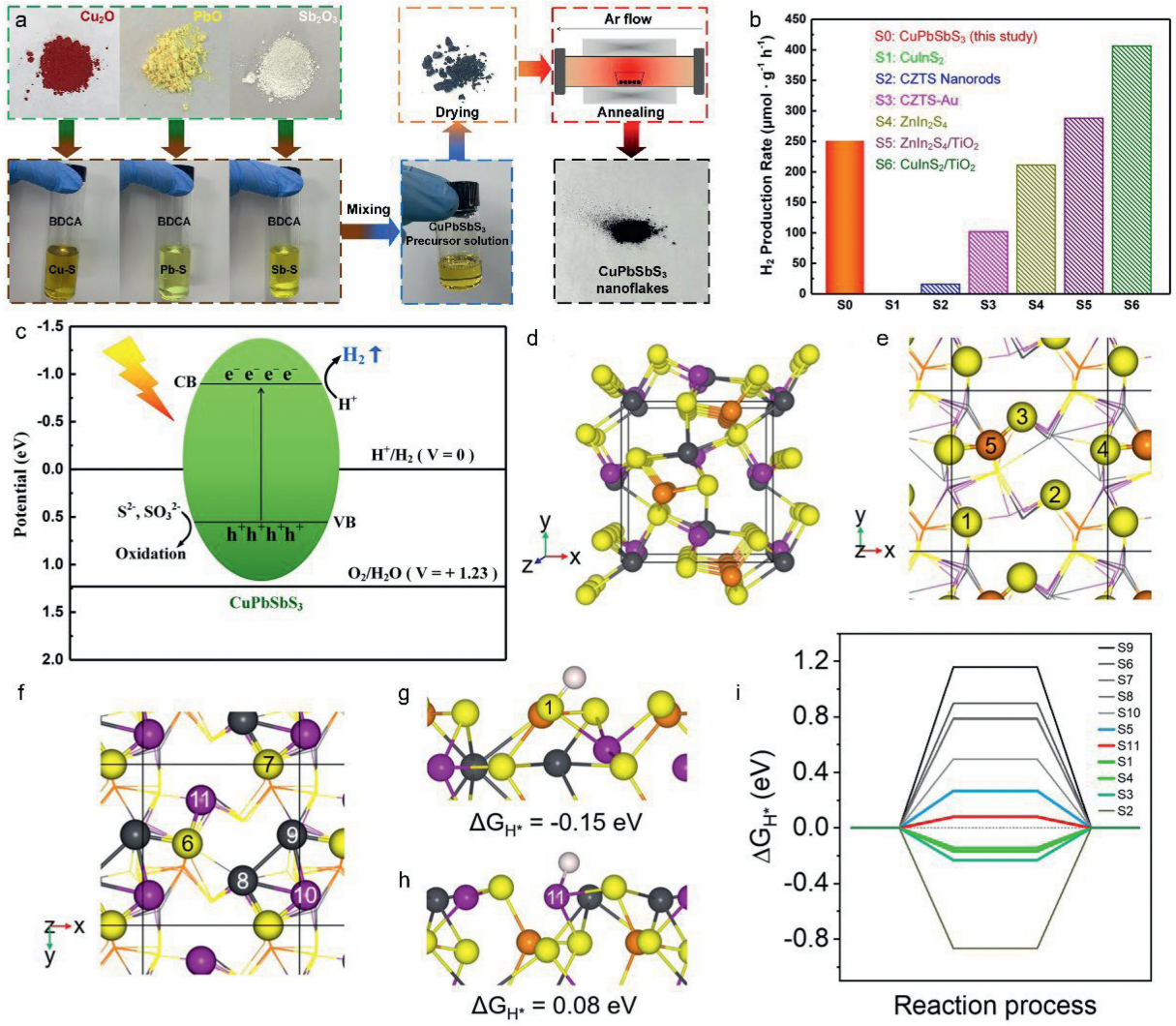

Fig. 5. (a) Fabrication process of $CuPbSbS_3$ nanoflakes through the BDCA solution method. (b) PHE rate and (c) the corresponding charge transfer mechanism of $CuPbSbS_3$ photocatalyst during the PHE process. (d–i) Theoritical hydrogen adorption energetics investigation on $CuPbSbS_3$ slab. Copied with permission [142]. Copyright 2022, Elsevier.

solution is a kind of mercapto acid production by the chemical reaction between *n*-butylamine and carbon disulfide [143]. In the room temperature, the BDCA solution can dissolve various kinds of metal oxides and metal hydroxide, forming the metal-sulfur-based precursor solution [143]. As shown in Fig. 5a, after dissolving the Cu_2O, PbO, and Sb_2O_3 in BDCA solution and mix them at a certain molar ratio, the $CuPbSbS_3$ can be obtained. After the subsequent drying and annealing process, the $CuPbSbS_3$ photocatalyst is finally synthesized. Under the simulated solar light irradiation, the PHE rate of $CuPbSbS_3$ photocatalyst was 250.8 μmol g^{-1} h^{-1}, which is comparable with some mature MMS under the same measurement condition, like $CuInS_2$ or $ZnIn_2S_4$ (Fig. 5b). According to the XPS valence band and UV–vis characterizations, the corresponding band potentials and charge transfer behaviors have also been proposed (Fig. 5c). Obviously, the negative band potential of $CuPbSbS_3$ reflect the strong HER driving force, which highlights the great PHE application potential of it. The promising PHE performance of $CuPbSbS_3$ photocatalyst was also confirmed by the density functional theory (DFT) calculations. Specifically, the lattice constants of $CuPbSbS_3$, calculated by the VASP, are $a = 7.91$ Å, $b = 8.22$ Å, and $c = 8.71$ Å, which are basically in agreement with the reported experimental values of $a = 7.81$ Å, $b = 8.15$ Å, and $c = 8.70$ Å (Fig. 5d). According to the characterization of high-resolution transmission electron microscopy (HRTEM), the exposed crystal plane of BDCA-synthesized $CuPbSbS_3$ photocatalyst is (002) and the corresponding S1–S11 absorption sites are shown in Figs. 5e and f. Moreover, the hydrogen adsorption configurations of S1 and S11 are shown in Figs. 5g and h. Based on the Gibbs-free energy of the adsorption of hydrogen atom ($\Delta G_H{}^*$) of S1–S11 (Fig. 5i), calculated by the DFT, the efficient PHE performance of $CuPbSbS_3$ photocatalyst was directly proved. Specifically, on the exposed (002) facet of $CuPbSbS_3$ nanoflakes, the unsaturated sulfur sites with nearly thermo-neutral $\Delta G_H{}^*$ are beneficial to adsorb and release hydrogen molecules, resulting in the finally efficient hydrogen production rate. Therefore, this work not only realized the synthesis of $CuPbSbS_3$ photocatalyst and applicated in photocatalysis but provided a clear research and analysis route.

4.2.3. $CuPbSbS_3$-based photocatalysts with further optimization

Similar to the development tendency of $CuSbS_2$, it also needs to adopt efficient strategies to improve the charge separation efficiency of $CuPbSbS_3$, aiming to enhance the photocatalytic performance. Recently, our group has successfully designed the $BiTiO_3/CuPbSbS_3$ heterostructure photocatalyst and realized the efficient piezo-photocatalytic degradation of RhB, which not only greatly enhanced the charge separation of bare $CuPbSbS_3$ but successfully broaden the photocatalytic application of $CuPbSbS_3$ from PHE to PD [144]. Concretely, the ferroelectric materials, with the

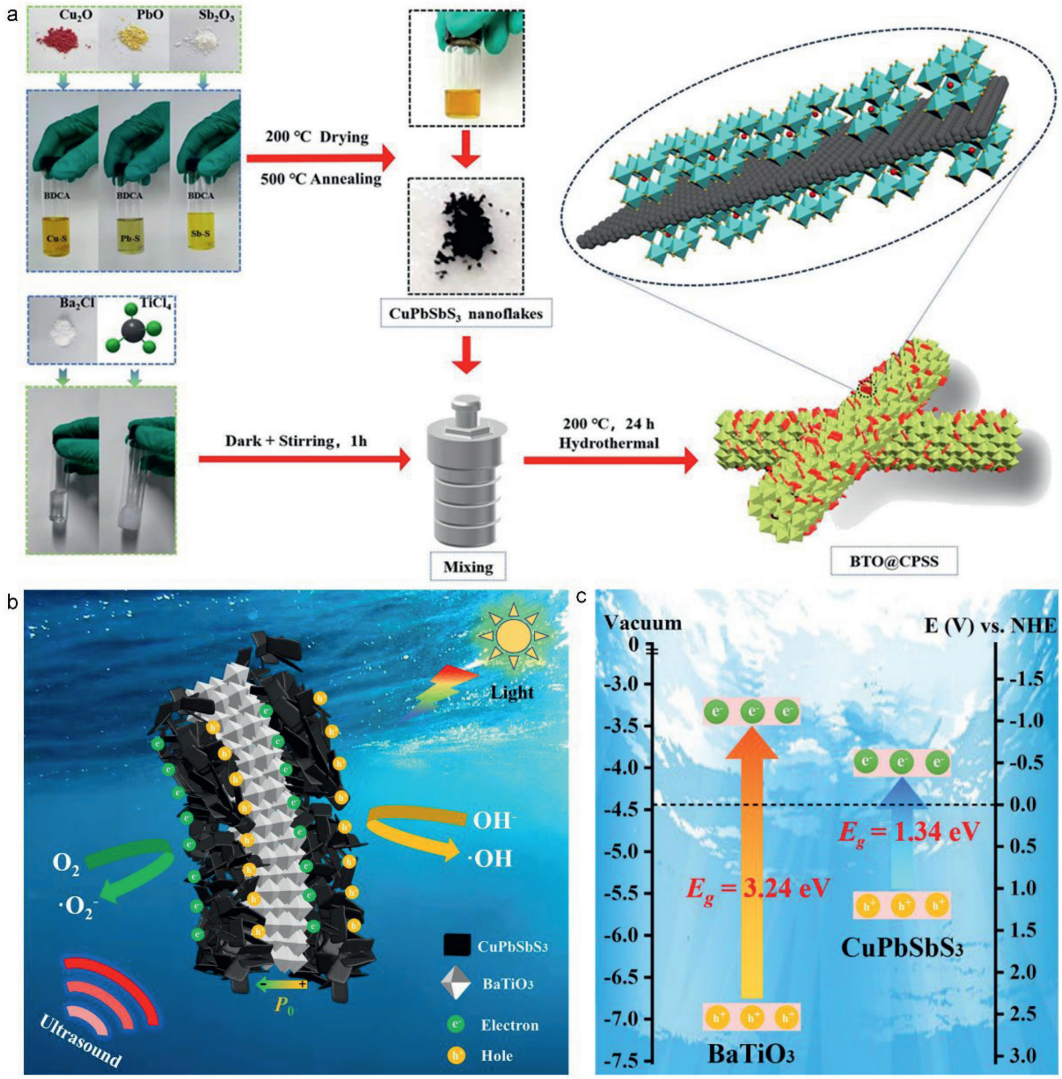

Fig. 6. (a) Fabrication process, (b) proposed mechanism, and (c) band structure of PD of RhB of $BiTiO_3$/$CuPbSbS_3$ photocatalyst. Copied with permission [144]. Copyright 2024, Elsevier.

structure feature of non-centrally symmetric, possess the unique property of spontaneous polarization. At the same time, the corresponding polarization direction can be reversed by the mechanical force or external electric field [145-152]. Typically, the $BiTiO_3$ with perovskite structure has achieved the most promising research progress in the exploration of ferroelectric materials due to its unique feature of natural piezoelectric and pyroelectric [153-157]. By tuning the mechanical force or temperature at the junction interface of the $BiTiO_3$-based heterostructure, the synergistic effect between $BiTiO_3$ and semiconductor photocatalysts can realize the enhancement of charges optoelectronic process. Specifically, the spontaneous polarizations of $BiTiO_3$ can generate an internal built-in electric field and thus provide an effective route for the construction with semiconductor photocatalyst with piezo/pyro-photoelectron effect, which has been demonstrated by the representative heterostructures of $BaTiO_3/TiO_2$ [158], $BaTiO_3/MoO_3$ [159], $BaTiO_3/Ag_2O$ [160], and $BaTiO_3$/C [155]. Taking the consideration of the unique semiconductor properties of $CuPbSbS_3$, it is speculated that the heterostructure of $BaTiO_3/CuPbSbS_3$ can also achieve a promising photocatalytic performance. As shown in Fig. 6a, on the basis of the BDCA-synthesized $CuPbSbS_3$, the $BiTiO_3/CuPbSbS_3$ heterostructure photocatalyst was further obtained through a conventional hydrothermal process. Based on the characterization of SEM and TEM, the $CuPbSbS_3$ nanoflakes tightly attach on the surface of $BiTiO_3$ nanorods, which is visually exhibited in the dashed ellipse Fig. 6a. In the heterostructure of $BiTiO_3/CuPbSbS_3$, the synergistic effect between the piezoelectricity feature of $BiTiO_3$ and semiconductor properties of $CuPbSbS_3$ can greatly improve the degradation-participating photogenerated holes density. Specifically, as shown in Figs. 6b and c, in the heterostructure of $BiTiO_3/CuPbSbS_3$, the $BiTiO_3$ can generate a piezoelectric field under the ultrasound, which is tending to perpendicular to the $BiTiO_3$ direction. Therefore, the photogenerated electrons and holes in $CuPbSbS_3$ can be effectively separated into opposite directions. Specifically, during the PD process, the reaction between the free charges and environment media can generate four major reactive oxygen species, namely hydroxyl radicals ($^{\bullet}OH$), hydrogen peroxide (H_2O_2), superoxide anion radical ($^{\bullet}O^{2-}$), and singlet oxygen ($^1O_2$) [161,162]. The corresponding PD reactions can be concluded as: $^{\bullet}O^{2-} + e^- + 2H^+ \rightarrow H_2O_2$; $H_2O_2 + e^- \rightarrow OH^- + {}^{\bullet}OH$. Among them, the $^1O_2$ possesses extremely short lifetime, which is the excited state of O_2. Therefore, the $^1O_2$ is generally absent in any PD reaction due to the easy quench [163]. In this case, the high density photogenerated holes, along with the $^{\bullet}OH$ and $^{\bullet}O_2^-$ directly participate in RhB degradation. Finally, under the further simulated solar light irradiation, the piezo-photocatalytic degrada-

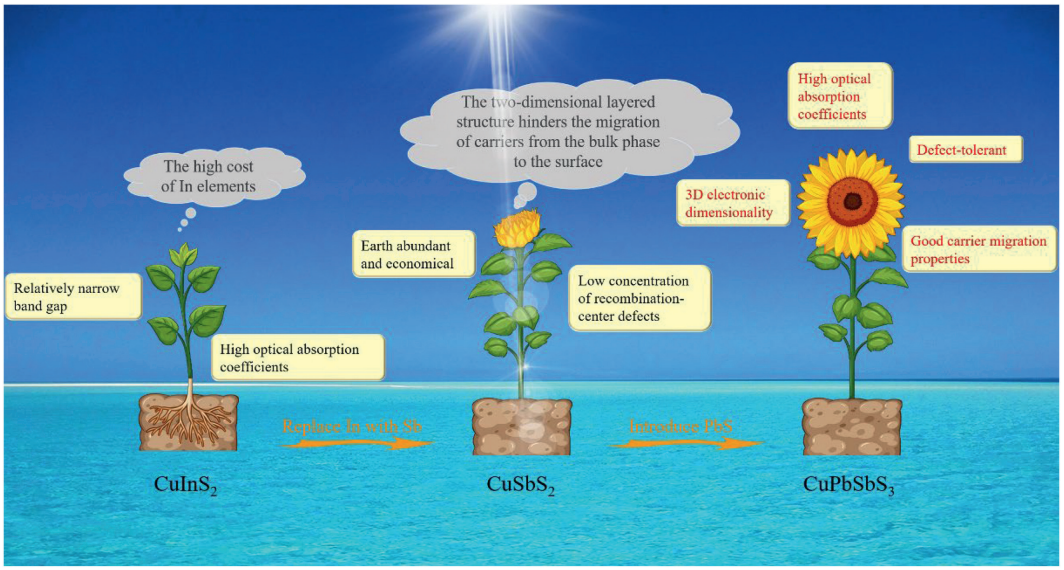

Fig. 7. The development tendency of Cu-based MMS photocatalysts: $CuInS_2 \rightarrow CuSbS_2 \rightarrow CuPbSbS_3$.

tion rate of RhB by $BiTiO_3/CuPbSbS_3$ heterostructure photocatalyst reached nearly 90.56% in only 0.5 h, along with a promising *k* value of 9.33×10^{-2} min^{-1}.

4.2.4. Summary of $CuPbSbS_3$ in photocatalytic applications

Promisingly, after incorporating the PbS into $CuSbS_2$, the restored photocatalyst of bournonite $CuPbSbS_3$ exhibits more excellent semiconductor properties, especially the direct bandgap, 3D crystal structure, and high electronic dimensionality, which can realize higher charge transfer efficiency and provide more active surface, and thus promote the final photocatalytic performance. Especially, the band width and isotropy of semiconductor photocatalyst can be strongly affected by the electronic dimensionality. Several representative researches have theoretically and experimentally proved that the high electronic dimensionality provides the opportunity to realize high-efficiency STE (although not guaranteeing) [76,89,99]. As expected, the photocatalyst of $CuPbSbS_3$ with excellent semiconductor features has preliminarily exhibited promising performance in photocatalysis, no matter in PHE or PD. However, the inherent drawback of $CuPbSbS_3$ is the existence of toxic Pb, which hinders the large-scale photocatalysis applications of it. In addition to the reported optimization strategies of mature MMS photocatalysts, like the controlling of the morphology and construction of heterojunction, future researches also need to focus on attempting other non-toxic element for the replacement of Pb without the loss of the semiconductor properties of $CuPbSbS_3$, which can further promote the development of MMS photocatalysts.

5. Discussion and outlooks

$CuSbS_2$ and $CuPbSbS_3$ are promising semiconductor materials in the application of photocatalysis. $CuSbS_2$ can significantly decrease the fabrication cost of $CuInS_2$ without the loss of semiconductor properties. Furthermore, bournonite $CuPbSbS_3$, the derivative of $CuSbS_2$, possesses more excellent semiconductor properties of 3D electronic dimensionality and defect-tolerant, which have greater potential to realize the efficient STE. Similar to the development in thin-film photovoltaics, $CuSbS_2$ and $CuPbSbS_3$-based photocatalysts have also been explored in photocatalytic applications of PHE and PD (Fig. 7 and Table S1 in Supporting information). Herein, the recent advances of $CuSbS_2$ and $CuPbSbS_3$-based photocatalysts for photocatalytic applications is timely reviewed, including the semiconductor properties of $CuSbS_2$ and $CuPbSbS_3$, basic mechanisms of PHE and PD, groundbreaking photocatalytic application of $CuSbS_2$ and $CuPbSbS_3$, and further photocatalytic performance optimization through heterojunction construction. However, compared with the mature MS photocatalysts, the corresponding explorations of $CuSbS_2$ and $CuPbSbS_3$ photocatalysts are still in the initial research stage. It still remains great space for the photocatalytic performance improvement based on the $CuSbS_2$ and $CuPbSbS_3$ photocatalysts and the understanding of the corresponding mechanisms. Moreover, some drawbacks and challenges of $CuSbS_2$ and $CuPbSbS_3$ photocatalysts in the current research stage also need to be considered. Specifically, $CuSbS_2$ and $CuPbSbS_3$ photocatalysts inevitably suffer from the photocorrosion phenomenon, which is also a general issue of MS photocatalysts. During the photocatalytic process, the photogenerated holes are easily combined with the S^{2-} under the light irradiation, resulting in the S^{2-} oxidized to sulfur [56]. As a result, the photostability is weakened due to the photocorrosion phenomenon. To date, several efficient strategies have been adopted to inhibit the photocorrosion phenomenon and thus enhance the photostability [26,45], mainly including combining passive metal on the surface of photocatalysts through loading, covering, and decorating; isolating the photocatalyst from the electrolyte through surface modification with carbon-based material, metal oxide, and polymer; and tuning the band energy by element doping. Another issue needs to be considered is the weak oxidizability. $CuSbS_2$ and $CuPbSbS_3$ photocatalysts have experimentally proved to own strong HER driving force due to the negative CB potential. Nevertheless, the negative VB potential leads to the weak oxidizability of photogenerated holes due to the narrow bandgap [54]. Current challenges and future research routes of $CuSbS_2$ and $CuPbSbS_3$-based photocatalysts mainly includes the followings:

(i) Controlling the morphology and design multifarious structures. For the semiconductor photocatalyst, the photocatalytic properties are not only determined by the species but by the morphologies and structures [164,165]. The strategies of controlling the morphology and design multifarious structures can provide larger specific surface area, which can supply more reaction active sites (Fig. 8). Meanwhile, the photogenerated charges separation can be boosted by reducing the gain size according to the equation of $\tau = r^2/\pi^2 D$, in

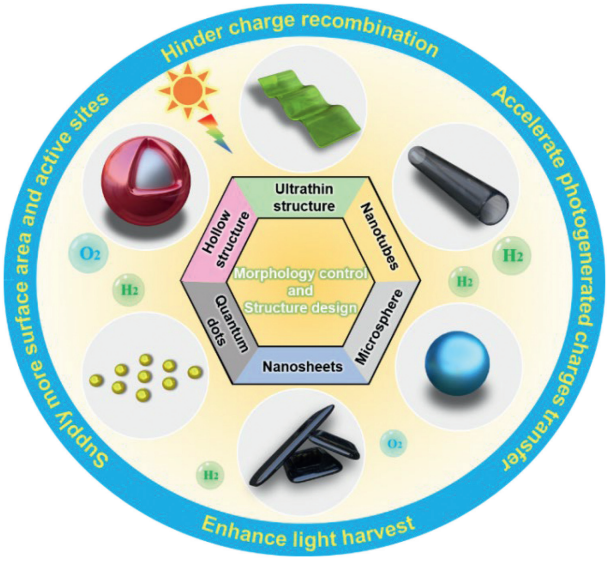

Fig. 8. Exhibition of several representative morphologies and structures of the reported MMS photocatalysts.

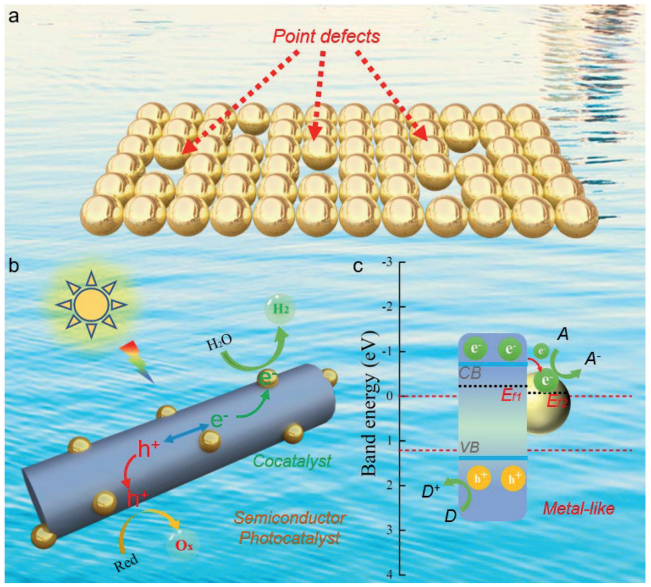

Fig. 9. Mechanism illustration of (a) point defects, (b) loading of cocatalysts, and (c) formation of Schottky junction.

which τ is the carriers' diffusion time from bulk to surface of the semiconductor photocatalyst, r is the radius of the gain, and D is the diffusion coefficient. Therefore, a higher surface-to-volume (STV) ratio can realize an enhanced photocatalytic performance, which have been proved by various photocatalysts, typically WO_3, Bi_2MoO_6, g-C_3N_4, CdS, $CuInS_2$, and $ZnIn_2S_4$. Notably, the currently synthesized $CuSbS_2$ and $CuPbSbS_3$ photocatalysts only contains vary limited morphologies of rods, dots, tetragonal particles, and nanoflakes due to the early-development stage. Referring to the deeper-explored photocatalysts, the diverse morphologies and structures need to be further focused, like the morphologies of nanowires, nanotubes, nanosheets, nanoflowers, covalent-organic framework (COF), microsphere, and nanoribbons; and the structures of core–shell, metal-organic framework (MOF), hollow structure, and quantum dots (QDs) [65-67]. Representatively, nanotubes own high STV ratio and better structure for higher light absorption efficiency [166]; hollow structure generally possesses rich surface active sites [167]; nanoflowers can significantly enhance the surface area [168]; nanosheets, especially the ultrathin nanosheets, can greatly enhance the separation efficiency of photogenerated electrons and holes, along with the low resistance and large surface [169,170]; and microspheres possess higher charge separation efficiency along with a reduced bandgap [171]. Especially, the semiconductor with a uniform nanocrystal distribution and crystal sizes of 2–10 nm is defined as QDs with the excellent semiconductor properties of size-dependent electronic performance, extended light absorption range, and quantum confinement effect, which is highly attracted in the current research of photocatalyst [172-178]. At the same time, by tuning the QD size, the bandgap of the QDs semiconductor can be optimized, and thus enhance the driving force of the charge transfer and the final photocatalytic performance. Moreover, the charge migration outside the QDs boundary also benefits from the quantum confinement effect of QDs. Therefore, the controlling of morphology and design of multifarious structures are great selective to improve the photocatalytic performance of semiconductor photocatalysts. In addition to broaden the morphologies and structures, the deep analysis of the charge transfer behaviors, thermal and mechanical stabilities, and photocatalytic mechanisms of the diverse morphologies and advanced structures are also important factors need to be improved, which are greatly meaningful for the broadened photocatalytic application of $CuSbS_2$ and $CuPbSbS_3$.

(ii) Introductions of vacancies. In the research field of STE, the vacancies in semiconductor photocatalysts are universally referred to "point defects" [179-182]. In general, the defects in semiconductor materials are regarded as the negative factor on the photocatalytic activity. The high-density defects can act as the recombination center and thus leads to the photogenerated charges recombination and decreased photocatalytic performance (Fig. 9a). However, after the optimization process, the defects with appropriate amount can be turned to take the positive effect on addressing the barrier of photocatalytic applications. Specifically, the optimal point defects (vacancies) in semiconductor photocatalyst can play the regulating functions for the photoelectrochemical and physicochemical features [183-185], resulting in the positive effects of accelerating photogenerated charges migration, improving surface active sites, and optimize the electronic band structure, which have been proved in the state-of-the-art photocatalysts. Nevertheless, the optimization of $CuSbS_2$ and $CuPbSbS_3$ photocatalysts through the vacancies has been rarely reported. Owing to the semiconductor properties of $CuSbS_2$ and $CuPbSbS_3$, especially the defect-tolerant property of $CuPbSbS_3$, it is greatly urgent to enhance the photocatalytic performance of $CuSbS_2$ and $CuPbSbS_3$ through the introduction of vacancies. In addition, the distribution of the concentration, generation process, deeper understanding of the fundamental functions, and existence state of the vacancies in $CuSbS_2$ and $CuPbSbS_3$ need to be further revealed to maximize the positive effects of the introduction of the vacancies.

(iii) Construction of advanced heterojunction. The construction of advanced $CuSbS_2$- and $CuPbSbS_3$-based heterojunction photocatalysts takes remarkable enhancement in improving charge separation efficiency and accelerating carriers' migration. During the exploration stage of MMS photocatalysts, the developed heterojunction types mainly include type-I,

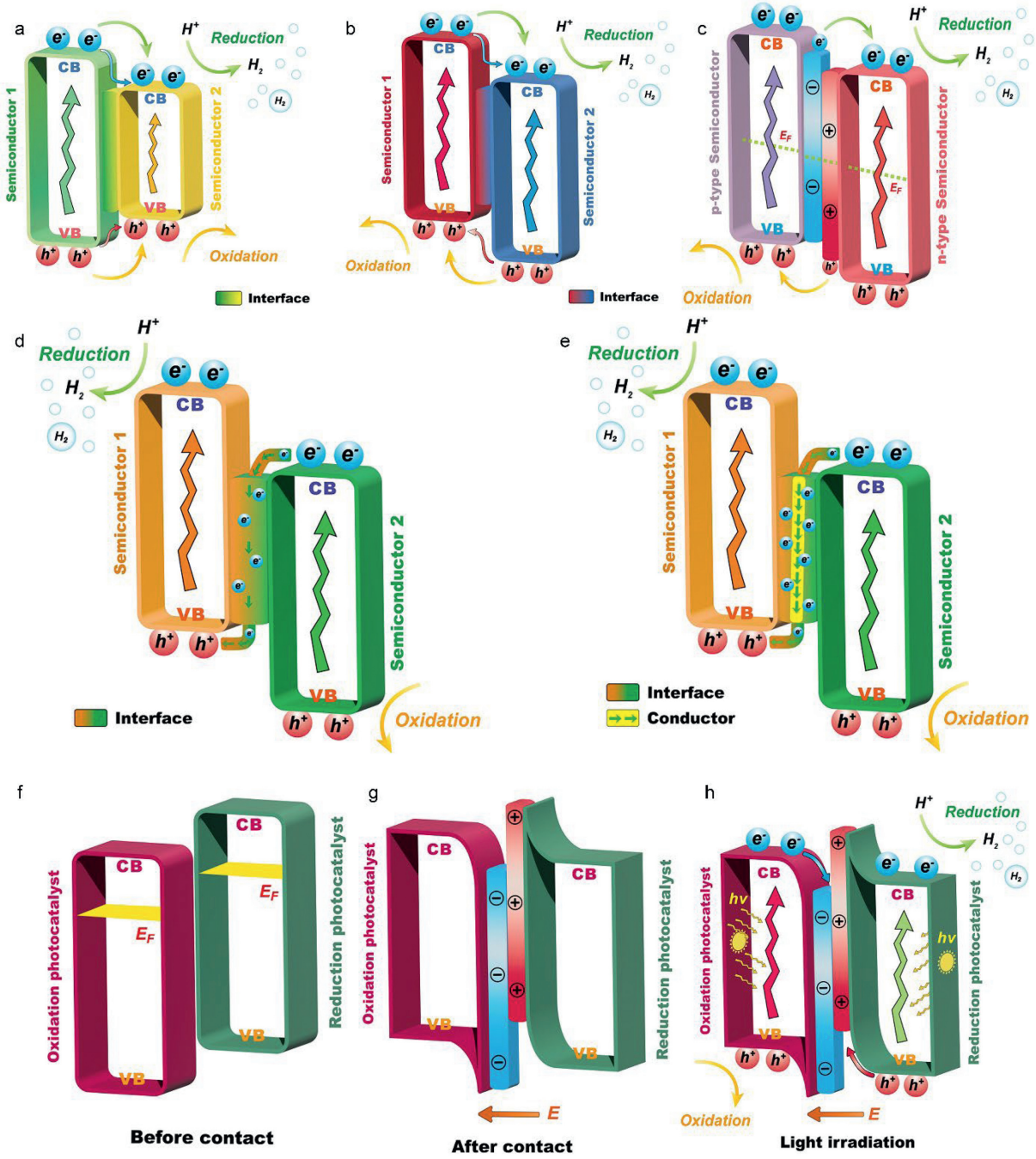

Fig. 10. Charge migration behaviors of the heterojunction types of (a) type-I, (b) type-II, (c) p-n, (d) Z-scheme without the electron mediator, and (e) Z-scheme with electron mediator. (f-h) Formation process of S-scheme heterojunction. Copied with permission [54]. Copyright 2024, Wiley Publishing Group.

type-II, p-n, Schottky, Z-scheme, and S-scheme heterojunctions (Figs. 9b and c, and 10) [19,24,112]. Interestingly, the typical BMS of MoS_2 is generally regarded as a kind of highly active photocatalyst due to the high catalytic surface and light absorption, which has also been proved in several representative studies [186-189]. Theoretically, compared with the later-explored MMS, MoS_2 possesses better potential and is more possible to achieve efficient photocatalytic performance through heterojunction construction. Practically, the experimentally synthesized MoS_2 photocatalyst is easily overlapped due to the stack layer or irregular aggregates of MoS_2 nanostructures. Moreover, the conductivity and active sites of MoS_2 photocatalyst are extremely difficult to precisely tune due to the presence of 1T' and 2H phases [63]. Although these issues can be solved by the synthesis of "monolayer MoS_2" [190], the corresponding technique difficulty and fabrication complexity are greatly increased. Therefore, compared with the mature BMS of MoS_2, the heterojunction construction based on MMS semiconductor materials has been paid more research attention. Up to now, the explored $CuSbS_2$- and $CuPbSbS_3$-based heterojunction photocatalysts mainly includes the types of type-I, type-II, and Z-scheme, which are also clearly exhibited in Figs. 4 and 6. Especially, the recently developed Z-scheme and S-scheme heterojunction have high-efficient charge separation and can effectively preserve the photogenerated electrons with

strong reducibility and the photogenerated holes with strong oxidizability, which is beneficial to realize the efficient photocatalytic performance [191-197]. Moreover, the Schottky junction, composed of one semiconductor photocatalyst and one metal-like material, can form a unique space-charge-separation region, which can also effectively promote the charge separation and migration [198]. The construction of Schottky junction with lower Fermi level (E_F) makes it easier for the photogenerated electrons migrate from the CB of the semiconductor photocatalyst from the metal-like material and directly participate in HER. In this case, the final PHE performance can be greatly enhanced due to the acceleration of the charge migration and prevention of photogenerated carriers' recombination. Therefore, further researches of $CuSbS_2$- and $CuPbSbS_3$-based heterojunction photocatalysts are still required and can be focused on the following aspects: constructing $CuSbS_2$ or $CuPbSbS_3$ with newly explored semiconductor materials with suitable band alignment, promising photoelectric and physicochemical properties; establishing the photogenerated charges transfer, migration, trapping, and recombination models through more powerful calculation and characterization methods (like *in-situ* characterization or machine learning) due to the importance of the dynamics of photogenerated charges during the photocatalytic process; and establishing more economical and facile experimental conditions to construct $CuSbS_2$- and $CuPbSbS_3$-based heterojunction photocatalysts through the advanced nanotechnology.

(iv) Exploring advanced synthesis methods. In addition to the photocatalysts of $CuSbS_2$ and $CuPbSbS_3$ mentioned in this review, most of the deep-researched MMS photocatalysts need to be synthesized under extra sulfur solution system. The generally applicated extra sulfur are Na_2S, thiourea, and thioacetamide [54,66]. The using of the extra sulfur not only increase the fabrication complexity but easily introduce high density sulfur vacancies, which are harmful for the final photocatalytic performance [61,183]. Moreover, the MMS photocatalysts synthesized under the extra sulfur system generally exist the photocorrosion phenomenon due to the unstable sulfur-based chemical bond adaptation environment [56], leading to a poor photostability during the photocatalytic process. Fortunately, these issues can be overcome by developing the sulfur-rich solution synthesis method to a certain extent, which can provide a relatively stable sulfur-based chemical bond adaptation environment and has been proved in several studies. Typically, the BDCA solution with the unique sulfur-rich feature, can effectively synthesize high-quality and stable MS photocatalyst without the using of extra sulfur [143]. Specifically, during the chemical reaction between *n*-butylamine ($C_4H_{11}N$) and carbon disulfide (CS_2), one of the C=S double bonds in CS_2 molecule is broken, forming the S=C−S− free radical. Then, the BDCA molecule ($C_5H_{11}NS_2$) can be formed due to the bonding of N− and H− with the unsaturated C− and S−. Therefore, due to the presence of thionothiolic acid group (−CSSH), the BDCA possesses the unique feature of sulfur-rich and can be ionized to the ions of H^+ and $C_5H_{10}NS_2^-$ by adding the buffer solutions, like ethanol or dimethylformamide, forming the sulfur-rich thionothiolic acid. At room temperature, the sulfur-rich BDCA solution can easily dissolve several kinds of MOs or metal hydroxides, generating the organometallic complex of $M(C_5H_{10}NS_2)_x$ and H_2O. Taking the further drying and annealing process, the extra sulfur and H_2O can be sublimated and the final MS photocatalyst with more stable M−S bonds and photostability can be synthesized by the decomposition of $M(C_5H_{10}NS_2)_x$. In addition to the BDCA-synthesized $CuPbSbS_3$ (Fig. 5a), the BDCA solution method has also successfully synthesized the MS photocatalyst of CdS and realized high-efficiency PHE performance without any cocatalyst and optimization strategies. Excitingly, in addition to the high PHE rate of 7.294 mmol g^{-1} h^{-1}, the hydrogen production emerges significance increasing during the long-time hydrogen production test due to the sulfur-rich synthesis process and activation of the photocatalyst [61]. Therefore, the BDCA solution method can not only decrease the fabrication complexity and decrease the extra sulfur vacancies but effectively overcome the issue of photocorrosion phenomenon to a certain extent, which is meaningful for further fabrication of advanced $CuSbS_2$- and $CuPbSbS_3$-based photocatalysts for efficient photocatalytic applications.

(v) *In situ* experimental characterization and deep theoretical calculations. Currently, the researches on $CuSbS_2$ and $CuPbSbS_3$ photocatalysts mainly focus on the generally experimental synthesis and DFT calculations. On this basis, deeper theoretical calculations, especially the machine learning, can further explore the chemistry spaces of the photocatalysts, which is meaningful to further design and explore advanced photocatalysts with excellent semiconductor properties [199]. As the pioneered photocatalyst, the TiO_2 is still widely researched in the current stage due to the earth-abundant and strong photostability. Typically, for the construction of TiO_2-based photocatalysts in PHE application, the accurate identification of the molecules on the surface of TiO_2 is the key factor. Representatively, this scientific topic has been performed by the machine learning of the dynamic simulation of the molecular, rather than the general calculation method of DFT [200]. In this dynamic simulation, the atomic energies of TiO_2, water, and TiO_2/water interface was predicted by the deep learning neural networks, which can effectively predict the atomic energies in the clusters. In this regard, the deep theoretical calculation of machine learning of the photocatalyst of TiO_2 in water splitting provide a meaningful research guidance of $CuSbS_2$ and $CuPbSbS_3$ in the photocatalytic applications. In another aspects, for various designed photocatalysts with modification strategies, the corresponding charge migration behaviors are not strictly proved due to the lack of *in situ* characterizations. Therefore, on the basis of machine learning, the accurate demonstration of improved photocatalytic activity through controlling the morphology and design multifarious structures, introductions of vacancies, and construction of heterojunctions, corresponding charge migration behaviors, and scientific design route will be deeper understood thought *in situ* characterizations [201-203].

(vi) Controlling of the reactive sites. For the photocatalytic process, the investigation of the morphology/structure-activity relationships between the reactive sites and the photocatalytic performance is greatly important. The sufficient reactive sites can be provided by controlling the experimental condition to tune the morphology or structure of the photocatalysts, resulting in the enhancement of the photocatalytic performance [204]. With reference to the reactive sites of MoS_2, the corresponding atomic structures of reactive sites of crystalline MoS_2 have been deeply researched. However, due to the diverse atomic structures of reactive sites in amorphous MoS_2, the corresponding HER mechanisms are still controversial. In this case, Hu *et al.* made a clear summarization of various HER mechanisms of amorphous MoS_2, surrounding the nature of reactive sites of them [205]. The corresponding nature of reactive sites mainly includes the identification and modification of sulfur atoms, and identi-

fication and coordination structure of Mo atoms. Similarly, Wang *et al*. realized the swapping of reactive sites from cationic Ni to anionic S in the hierarchical structure photocatalyst of NiS_2/NiS_2-NiS (NiS_2 nanoflowers grown on dual-phased NiS_2-NiS foam) [206], demonstrating the remarkably antidromic electron transfer from the reactive site of Ni to S. In this case, the adsorption of hydrogen species is effectively relieved and higher intrinsic activity at the reactive site of S over Ni is also endowed. Moreover, the reactive sties engineering in the heterostructure and single atoms catalysts in photocatalytic application, especially in PHE, have also been deeply studied [207,208]. Therefore, based on the above researches, future researches of $CuSbS_2$- and $CuPbSbS_3$-based photocatalysts can also focus on the engineering of the reactive sites, aiming to further realize the enhancement of the photocatalytic performance.

In addition to the modification strategies mentioned above, some recently explored methods and reported reviews are highly meaningful for further development of $CuSbS_2$- and $CuPbSbS_3$-based photocatalysts in the aspect of the significance of sulfur. Representatively, Li *et al*. designed the electrocatalyst of CN@NiCoS (nickel-cobalt sulfides heterostructure with nitrogen-doped carbon shell) and clearly identified the corresponding sulfur migration, aiming to overcome the activity-stability trade-offs in MS catalysts [209]. At the heterointerface of Ni_3S_2-Co_9S_8, the sulfur migration can be greatly stimulated due to the creation of the sulfur vacancies. At the same time, the CN shell can directly capture the migrated sulfur atoms *via* the strong C−S bond, which effectively avoids the dissolution of sulfide into the alkaline electrolyte. Therefore, in the aspect of the significance of sulfur, this work provides an advanced design concept of HER electrocatalyst through interfacial atomic migration engineering. Similarly, Cai *et al*. designed the MoS_2/MS heterostructure *via* the metal-sulfur bond and took it into the application of photocatalytic CO_2 reduction [210]. Especially in the MoS_2/In_2S_3 heterostructure, both MoS_2 and In_2S_3 exhibited the same lamellar morphology, resulting in a high specific surface area and favorable environment for the formation of build-in electric field. Moreover, the excitement of the carriers can be also promoted due to the small gap between VB minimum and E_F in the MoS_2/In_2S_3 heterostructure, and thus synthetically enhance the photocatalytic CO_2 reduction performance. Also, in the field of photocatalytic CO_2 reduction, the Co-based co-catalysts for the enhancement of the photocatalytic performance was also systematically summarized [211]. Hence, the above advanced researches provide clear directions for the further design of $CuSbS_2$- and $CuPbSbS_3$-based photocatalysts. Meanwhile, the scientific research route of $CuSbS_2$- and $CuPbSbS_3$-based photocatalysts can also refer to the hot research photocatalysts in the current stage, like COF, MOF, and g-C_3N_4. For these hot research photocatalysts, the corresponding advanced modification strategies generally contain amorphous single atom or diatomic loading [212-216], van der Waals heterojunction [217-220], microenvironment regulation [221], and spin state regulation [222,223], which have successfully and effectively enhanced the photocatalytic performance of COF, MOF, and g-C_3N_4 in the photocatalytic applications of hydrogen production, pollution degradation, carbon dioxide reduction, nitrogen fixation, and oxygen reduction. Moreover, the strategy combination of amorphous 2D layered structure with others also take great positive effects on the photocatalytic performance enhancement of COF, MOF, and g-C_3N_4 photocatalysts. Typically, the amorphous 2D layered structure with van der Waals heterojunction construction possesses the unique merits of the followings [219]: (i) Effective interactions and wide interface area with the "face to face" contact type; (ii) tunable bandgap of 2D structure with broaden light absorption range; (iii) hindered charge recombination and enhanced carriers' migration between the amorphous 2D layers; (iv) appropriate electronic coupling between the 2D layers with optimized electronic band structure. For the photocatalysts with amorphous 2D layered structure, apart from the combination of van der Waals heterojunction construction, other combined strategies have also taken the positive effects on the photocatalytic performance enhancement of COF, MOF, and g-C_3N_4 photocatalysts. Hence, the research experience of mature photocatalysts of COF, MOF, and g-C_3N_4 is also beneficial for the future researches of $CuSbS_2$ and $CuPbSbS_3$ photocatalysts, aiming to realize further improvement of photocatalytic applications.

In summary, $CuSbS_2$ and its derivative of $CuPbSbS_3$ are earth-abundant and stable semiconductor materials and exhibit promising photoelectric and semiconductor properties, indicating great potential for STE applications. The PHE and PD applications have been preliminarily explored based on the photocatalysts of $CuSbS_2$ and $CuPbSbS_3$ and achieved promising progresses and excellent photocatalytic performance, revealing the great application potential of $CuSbS_2$ and $CuPbSbS_3$ photocatalysts. It is expected that the future researches will achieve groundbreakings with respect to the photocatalytic performance. With the deepening of future research, $CuSbS_2$ and its derivative of $CuPbSbS_3$ are expected to hot topics in case of photocatalytic techniques.

Declaration of competing interest

The authors declare that they have no known competing financial interests or personal relationships that could have appeared to influence the work reported in this paper.

CRediT authorship contribution statement

Xinlong Zheng: Writing – original draft, Conceptualization. **Zhongyun Shao:** Validation. **Jiaxin Lin:** Supervision. **Qizhi Gao:** Supervision. **Zongxian Ma:** Supervision. **Yiming Song:** Supervision. **Zhen Chen:** Supervision. **Xiaodong Shi:** Supervision. **Jing Li:** Supervision. **Weifeng Liu:** Supervision. **Xinlong Tian:** Writing – review & editing, Writing – original draft, Project administration. **Yuhao Liu:** Writing – review & editing, Writing – original draft, Project administration, Data curation, Conceptualization.

Acknowledgments

This work was supported by the National Natural Science Foundation of China (Nos. 22109034, 22109035, 52164028, 62105083, 22202053, 52304326, 22309037, 22305055, 52362010), the Start-up Research Foundation of Hainan University (Nos. KYQD(ZR)-20008, 20082, 20083, 20084, 21065, 21124, 21125), the Innovative Research Projects for Graduate Students of Hainan Province (No. Qhyb2023-20), the Collaborative Innovation Center of Marine Science and Technology of Hainan University (No. XTCX2022HYC21), the first batch of "Nanhai New Star" Industrial Innovation Talent Platform Project (No. NHXXRCXM202309006), and the specific research fund of The Innovation Platform for Academicians of Hainan Province. The authors acknowledge the support for comprehensive characterizations by Pico Election Microscopy Center of Hainan University.

Supplementary materials

Supplementary material associated with this article can be found, in the online version, at doi:10.1016/j.cclet.2024.110533.

References

[1] X. Li, Y. Ma, Y. Yue, et al., Chem. Eng. J. 428 (2022) 130965.
[2] Y. Zhao, M. Hu, H. Li, et al., J. Mater. Chem. A 10 (2022) 18609–18615.

[3] M. Wang, Y. Cheng, H. Zhang, et al., Adv. Funct. Mater. 33 (2023) 2211199.
[4] S. Zhao, X. Luo, Y. Cheng, et al., Chem. Eng. J. 454 (2023) 140360.
[5] Y. Yue, N. Liu, T. Su, et al., Adv. Funct. Mater. 33 (2023) 2211613.
[6] C. Zhou, L. Shan, Q. Nan, et al., Adv. Funct. Mater. 23 (2024) 2312696.
[7] H. Tian, D. Wu, J. Li, et al., J. Energy Chem. 70 (2022) 230–235.
[8] P. Rao, D. Wu, T.J. Wang, et al., eScience 2 (2022) 399–404.
[9] X. Li, X. Wu, Y. Zhao, et al., Adv. Mater. 35 (2023) 2302467.
[10] D. Xing, W. Pan, Z. Xie, et al., Mater. Lett. 327 (2022) 133079.
[11] P. Rao, J. Luo, J. Li, et al., Carbon Energy 4 (2022) 1003–1010.
[12] J. Chen, X. Shi, S. Feng, et al., Nano Mater. Sci. 6 (2024) 413–418.
[13] Y. Song, W. Xie, M. Shao, X. Duan, Nano Mater. Sci. 5 (2023) 161–176.
[14] Q.S. Jiang, W. Cheng, J. Wu, et al., Electrochim. Acta 324 (2019) 134896.
[15] J. Guo, S. Chen, Y. Xu, et al., J. Colloid Interface Sci. 624 (2022) 629–636.
[16] D. Liu, Y. Zhao, C. Wu, et al., Nano Energy 98 (2022) 107296.
[17] A.L. Linsebigler, G. Lu, J.T. Yates Jr., Chem. Rev. 95 (1995) 735–758.
[18] A.J. Esswein, D.G. Nocera, Chem. Rev. 107 (2007) 4022–4047.
[19] A. Kudo, Y. Miseki, Chem. Soc. Rev. 38 (2009) 253–278.
[20] X. Chen, S. Shen, L. Guo, S.S. Mao, Chem. Rev. 110 (2010) 6503–6570.
[21] J. Ran, J. Zhang, J. Yu, et al., Chem. Soc. Rev. 43 (2014) 7787–7812.
[22] X. Yang, D. Wang, ACS Appl. Energy Mater. 1 (2018) 6657–6693.
[23] H. Wang, H. Wang, Z. Wang, et al., Chem. Soc. Rev. 49 (2020) 4135–4165.
[24] C. Cheng, B. He, J. Fan, et al., Adv. Mater. 33 (2021) 2100317.
[25] X. Tao, Y. Zhao, S. Wang, et al., Chem. Soc. Rev. 51 (2022) 3561–3608.
[26] S. Chandrasekaran, L. Yao, L. Deng, et al., Chem. Soc. Rev. 48 (2019) 4178–4280.
[27] J.S. O'Neill, L. Kearney, M.P. Brandon, M.T. Pryce, Coord. Chem. Rev. 467 (2022) 214599.
[28] Z. Liang, Y. Xue, X. Wang, et al., Nano Mater. Sci. 5 (2023) 202–209.
[29] B. Ge, C. Li, W. Lu, et al., Adv. Energy Mater. 13 (2023) 2300965.
[30] Y. Zhi, C. Gu, H. Ji, et al., Chin. Chem. Lett. 36 (2025) 110234.
[31] A. Fujishima, K. Honda, Nature 238 (1972) 37–38.
[32] B. Wei, M. Calatayud, Catal. Today 397-399 (2022) 113–120.
[33] D. Zhao, C.F. Yang, Renew. Sustain. Energy Rev. 54 (2016) 1048–1059.
[34] R. Asahi, T. Morikawa, T. Ohwaki, et al., Science 293 (2001) 269–271.
[35] D. Gao, H. Long, X. Wang, et al., Adv. Funct. Mater. 33 (2023) 2209994.
[36] Y. Li, Y. Wei, W. He, et al., Chin. Chem. Lett. 34 (2023) 108417.
[37] Z. Li, R. Li, H. Jing, et al., Nat. Catal. 6 (2023) 80–88.
[38] G. Liu, S. Li, Y. Lu, et al., J. Alloys Compd. 689 (2016) 787–799.
[39] D.P.H. Tran, M.T. Pham, X.T. Bui, et al., Sol. Energy 240 (2022) 443–466.
[40] P. Shandilya, S. Sambyal, R. Sharma, et al., J. Hazard. Mater. 428 (2022) 128218.
[41] S. Patial, V. Hasija, P. Raizada, et al., J. Environ. Chem. Eng. 8 (2020) 103791.
[42] A. Malathi, J. Madhavan, M. Ashokkumar, P. Arunachalam, Appl. Catal. A 555 (2018) 47–74.
[43] H. Raebiger, S. Lany, A. Zunger, Phys. Rev. B 76 (2007) 045209.
[44] E. Pastor, M. Sachs, S. Selim, et al., Nat. Rev. Mater. 7 (2022) 503–521.
[45] Q. Zhu, Q. Xu, M. Du, et al., Adv. Mater. 34 (2022) 2202929.
[46] K. Zhang, L. Guo, Catal. Sci. Technol. 3 (2013) 1672–1690.
[47] M.D. Regulacio, M.Y. Han, Acc. Chem. Res. 49 (2016) 511–519.
[48] D. Huang, M. Wen, C. Zhou, et al., Appl. Catal. B 267 (2020) 118651.
[49] J. Xu, W. Zhong, X. Zhang, et al., Small 19 (2023) 2303960.
[50] Y. Liu, X. Zheng, Y. Yang, et al., Solar RRL 6 (2022) 2101061.
[51] X. Zheng, Y. Yang, Y. Liu, et al., Rare Met. 41 (2022) 2153–2168.
[52] T. Di, Q. Xu, W. Ho, et al., ChemCatChem 11 (2019) 1394–1411.
[53] D. Gao, J. Xu, L. Wang, et al., Adv. Mater. 34 (2022) 2108475.
[54] Y. Song, X. Zheng, Y. Yang, et al., Adv. Mater. 36 (2024) 2305835.
[55] Y. Yu, S.Y. Huang, Y. Li, et al., Nano Lett. 14 (2014) 553–558.
[56] S. Chen, C. Li, K. Domen, F. Zhang, Joule 7 (2023) 1–23.
[57] X. Zheng, Y. Liu, Y. Yang, et al., Renewables 1 (2023) 39–56.
[58] R. Shen, D. Ren, Y. Ding, et al., Sci. China Mater. 63 (2020) 2153–2188.
[59] J.A. Nasir, Z.u. Rehman, S.N.A. Shah, et al., J. Mater. Chem. A 8 (2020) 20752–20780.
[60] B. Chai, M. Xu, J. Yan, Z. Ren, Appl. Surf. Sci. 430 (2018) 523–530.
[61] X. Zheng, Y. Song, Y. Liu, et al., Small 19 (2023) 2207623.
[62] H. Deng, Y. Cheng, Z. Chen, et al., Adv. Funct. Mater. 33 (2023) 2212627.
[63] L. Zheng, F. Teng, X. Ye, et al., Adv. Energy Mater. 10 (2020) 1902355.
[64] Y. Liu, X. Zheng, Y. Yang, et al., ChemCatChem 14 (2022) e202101439.
[65] X. Zheng, Y. Yang, Y. Song, et al., Interdiscip. Mat. 2 (2023) 669–688.
[66] X. Zheng, Y. Song, Y. Liu, et al., Coord. Chem. Rev. 475 (2023) 214898.
[67] Y. Yang, X. Zheng, Y. Song, et al., Int. J. Hydrogen Energy 48 (2023) 3791–3806.
[68] A.W. Welch, P.P. Zawadzki, S. Lany, et al., Sol. Energy Mater. Sol. Cells 132 (2015) 499–506.
[69] B. Krishnan, S. Shaji, R.Ernesto Ornelas, J. Mater. Sci.: Mater. Electron. 26 (2015) 4770–4781.
[70] K. Ramasamy, H. Sims, W.H. Butler, A. Gupta, J. Am. Chem. Soc. 136 (2014) 1587–1598.
[71] A.W. Welch, L.L. Baranowski, P. Zawadzki, et al., Prog. Photovoltaics 24 (2016) 929–939.
[72] S. Gautam, H. Agrawal, M. Thakur, et al., J. Environ. Chem. Eng. 8 (2020) 103726.
[73] S. Tasleem, M. Tahir, Renew. Sustain. Energy Rev. 132 (2020) 110073.
[74] K.S. Schanze, P.V. Kamat, P. Yang, J. Bisquert, ACS Energy Lett. 5 (2020) 2602–2604.
[75] G. Zhang, G. Liu, L. Wang, J.T.S. Irvine, Chem. Soc. Rev. 45 (2016) 5951–5984.
[76] Y. Liu, B. Yang, M. Zhang, et al., Nano Energy 71 (2020) 104574.
[77] L. Wan, C. Ma, K. Hu, et al., J. Alloys Compd. 680 (2016) 182–190.
[78] F.W. de Souza Lucas, A.W. Welch, L.L. Baranowski, et al., J. Phys. Chem. C 120 (2016) 18377–18385.
[79] L. Fu, J. Yu, J. Wang, et al., Chem. Eng. J. 400 (2020) 125906.
[80] P.K.Singh Sadanand, S. Rai, et al., Sol. Energy 222 (2021) 175–185.
[81] M. Zhang, Y. Liu, B. Yang, et al., ACS Appl. Mater. Interfaces 13 (2021) 13273–13280.
[82] A. Sarilmaz, E. Genc, E. Aslan, et al., J. Photochem. Photobiol. A 400 (2020) 112706.
[83] R. Yang, L. Mei, Y. Fan, et al., Small Methods 5 (2021) 2100887.
[84] J. Wang, S. Sun, R. Zhou, et al., J. Mater. Sci. Technol. 78 (2021) 1–19.
[85] R. Janani, R. Preethi V, S. Singh, et al., Catalysts 11 (2021) 277.
[86] T. Zhang, T. Wang, F. Meng, et al., J. Mater. Chem. C 10 (2022) 5400–5424.
[87] Y. Kumar, R. Kumar, P. Raizada, et al., J. Mater. Sci. Technol. 87 (2021) 234–257.
[88] A. Walsh, D.J. Payne, R.G. Egdell, G.W. Watson, Chem. Soc. Rev. 40 (2011) 4455–4463.
[89] Z. Xiao, W. Meng, J. Wang, et al., Mater. Horiz. 4 (2017) 206–216.
[90] S. Duan, Y. Cheng, W. Xia, et al., Nature 595 (2021) 239–244.
[91] Y. Wu, N.H. Jo, D. Mou, et al., Phys. Rev. B 95 (2017) 195138.
[92] S. Cho, B.S. Kim, B. Kim, et al., Phys. Chem. Chem. Phys. 20 (2018) 23007–23012.
[93] T.D. Lee, A.U. Ebong, Renew. Sustain. Energy Rev. 70 (2017) 1286–1297.
[94] Y. Wang, G. Wang, Y. Zhou, et al., Renew. Sustain. Energy Rev. 183 (2023) 113427.
[95] Y. Rong, Y. Hu, A. Mei, et al., Science 361 (2018) eaat8235.
[96] Y. Wu, M. Wei, Y. Sun, et al., Vacuum 222 (2024) 113057.
[97] Y. Bai, D. Xing, H. Luo, et al., Appl. Surf. Sci. 552 (2021) 149459.
[98] Q.S. Jiang, Z. Xie, M. Wei, et al., Mater. Lett. 355 (2024) 135485.
[99] S. Geng, Z. Xiao, ACS Energy Lett. 8 (2023) 2051–2057.
[100] R. Wu, Y. Liu, S. Hu, et al., Adv. Optical Mater. 10 (2022) 2201081.
[101] Z. Xiao, Z. Song, Y. Yan, Adv. Mater. 31 (2019) 1803792.
[102] Z. Xie, Y. Wu, M. Wei, et al., ChemistrySelect 8 (2023) e202300082.
[103] Z. Xiao, Y. Yan, Adv. Energy Mater. 7 (2017) 1701136.
[104] Q.S. Jiang, Y. Wu, Z. Xie, et al., Mater. Today Commun. 35 (2023) 106401.
[105] S. Chen, W. Liu, M. Xu, et al., J. Mater. Chem. C 11 (2023) 8431–8437.
[106] Q. Sun, B. Ge, B. Xiao, et al., Adv. Sci. 10 (2023) 2302236.
[107] B. Yang, L. Wang, J. Han, et al., Chem. Mater. 26 (2014) 3135–3143.
[108] P. Makuła, M. Pacia, W. Macyk, J. Phys. Chem. Lett. 9 (2018) 6814–6817.
[109] Z. Wei, J. Liu, W. Shangguan, Chin. J. Catal. 41 (2020) 1440–1450.
[110] K. Pingmuang, J. Chen, W. Kangwansupamonkon, et al., Sci. Rep. 7 (2017) 8929.
[111] Y. Zhang, Y. Zhang, H. Zhang, et al., Coord. Chem. Rev. 448 (2021) 214147.
[112] J. Low, J. Yu, M. Jaroniec, et al., Adv. Mater. 29 (2017) 1601694.
[113] L. Zhang, J. Zhang, H. Yu, J. Yu, Adv. Mater. 34 (2022) 2107668.
[114] W. Xue, D. Huang, X. Wen, et al., J. Hazard. Mater. 390 (2020) 122128.
[115] B. Qiu, L. Cai, N. Zhang, et al., Adv. Sci. 7 (2020) 1903568.
[116] W. Wang, Q. Sheng, G. Zhi, et al., Appl. Surf. Sci. 639 (2023) 158251.
[117] G. Zhi, L. Hao, W. Chen, et al., ChemistrySelect 7 (2022) e202202457.
[118] G. Zhi, W. Wang, M. Zhang, et al., J. Mater. Sci. Mater. Electron. 31 (2020) 17036–17043.
[119] M. Frumar, T. Kala, J. Horák, J. Cryst. Growth 20 (1973) 239–244.
[120] Y.T. Alharbi, F. Alam, K. Parvez, et al., Inorg. Chem. 60 (2021) 13691–13698.
[121] K.M. Koskela, B.C. Melot, R.L. Brutchey, J. Am. Chem. Soc. 142 (2020) 6173–6179.
[122] A. Faghaninia, G. Yu, U. Aydemir, et al., Phys. Chem. Chem. Phys. 19 (2017) 6743–6756.
[123] L. Lin, R. Da, C. Zheng, et al., Crystals 13 (2023) 1256.
[124] C. Yan, F. Liu, K. Sun, et al., Sol. Energy Mater. Sol. Cells 144 (2016) 700–706.
[125] W. Wang, M.T. Winkler, O. Gunawan, et al., Adv. Energy Mater. 4 (2014) 1301465.
[126] Z. Su, K. Sun, Z. Han, et al., J. Mater. Chem. A 2 (2014) 500–509.
[127] P. Xu, S. Chen, B. Huang, et al., Phys. Rev. B 88 (2013) 045427.
[128] Y. Cao, M.S. Denny Jr., J.V. Caspar, et al., J. Am. Chem. Soc. 134 (2012) 15644–15647.
[129] S. Chen, A. Walsh, X.G. Gong, S.H. Wei, Adv. Mater. 25 (2013) 1522–1539.
[130] L. Zhu, Y.H. Qiang, Y.L. Zhao, X.Q. Gu, Appl. Surf. Sci. 292 (2014) 55–62.
[131] H. Deng, Q. Sun, Z. Yang, et al., Nat. Commun. 12 (2021) 3107.
[132] Q. Sun, C. Shi, W. Xie, et al., Adv. Sci. 11 (2024) 2306740.
[133] Z. Zhao, C. Ma, Y. Cao, et al., Phys. Lett. A 377 (2013) 417–422.
[134] D. Yokoyama, T. Minegishi, K. Jimbo, et al., Appl. Phys. Express 3 (2010) 101202.
[135] G. Ma, T. Minegishi, D. Yokoyama, et al., Chem. Phys. Lett. 501 (2011) 619–622.
[136] S.C. Riha, S.J. Fredrick, J.B. Sambur, et al., ACS Appl. Mater. Interfaces 3 (2011) 58–66.
[137] L. Wang, W. Wang, S. Sun, J. Mater. Chem. 22 (2012) 6553–6555.
[138] Z.X. Chang, W.H. Zhou, D.X. Kou, et al., Chem. Commun. 50 (2014) 12726–12729.
[139] N. Guijarro, M.S. Prevot, K. Sivula, J. Phys. Chem. Lett. 5 (2014) 3902–3908.
[140] E. Ha, L.Y. Lee, J. Wang, et al., Adv. Mater. 26 (2014) 3496–3500.
[141] Z.X. Chang, R.F. Chong, Y.N. Meng, et al., Int. J. Hydrogen Energy 40 (2015) 13456–13462.
[142] X. Zheng, D. Wu, Y. Liu, et al., Mater. Today Energy 25 (2022) 100956.
[143] Y. Liu, C. Chen, Y. Zhou, et al., J. Mater. Chem. C 7 (2019) 11068–11084.
[144] Z. Chen, G. Li, X. Zheng, et al., Nano Energy 124 (2024) 109463.

[145] N. Ma, C. Lu, Y. Liu, et al., Small 20 (2024) 2304839.
[146] B. Tian, R. Tian, S. Liu, et al., Adv. Mater. 35 (2023) 2304262.
[147] W. Amdouni, M. Fricaudet, M. Otoničar, et al., Adv. Mater. 35 (2023) 2301841.
[148] M.L. Xu, M. Lu, G.Y. Qin, et al., Angew. Chem. Int. Ed. 61 (2022) e202210700.
[149] R. Mohanty, S. Mansingh, K. Parida, K. Parida, Mater. Horiz. 9 (2022) 1332–1355.
[150] S. Dutta, P. Buragohain, S. Glinsek, et al., Nat. Commun. 12 (2021) 7301.
[151] Y. Liu, S. Ye, H. Xie, et al., Adv. Mater. 32 (2020) 1906513.
[152] Z. Liu, L. Wang, X. Yu, et al., Adv. Funct. Mater. 29 (2019) 1807279.
[153] S. Xu, L. Guo, Q. Sun, Z.L. Wang, Adv. Funct. Mater. 29 (2019) 1808737.
[154] J. Wei, J. Xia, X. Liu, et al., Appl. Catal. B 328 (2023) 122520.
[155] H. Zheng, X. Li, K. Zhu, et al., Nano Energy 93 (2022) 106831.
[156] X. Zhou, S. Wu, C. Li, et al., Nano Energy 66 (2019) 104127.
[157] T. Wang, J. Cao, J. Li, et al., Chin. Chem. Lett. 36 (2025) 110078.
[158] B. Fu, J. Li, H. Jiang, et al., Nano Energy 93 (2022) 106841.
[159] K.V. Alex, A. Prabhakaran, A.R. Jayakrishnan, et al., ACS Appl. Mater. Interfaces 11 (2019) 40114–40124.
[160] W. Zhao, Q. Zhang, H. Wang, et al., Nano Energy 73 (2020) 104783.
[161] J. Zhang, R. Balasubramanian, X. Yang, Chem. Eng. J. 453 (2023) 139776.
[162] Y. Bai, S. Li, B. Yin, et al., Trans. Tianjin Univ. 30 (2024) 130–139.
[163] Y. Nosaka, A.Y. Nosaka, Chem. Rev. 117 (2017) 11302–11336.
[164] K. Han, G. Dong, I. Saeed, et al., Chin. J. Struct. Chem. 43 (2024) 100208.
[165] K. Mishra, N. Devi, S.S. Siwal, et al., Adv. Sustain. Syst. 7 (2023) 2300095.
[166] H. Yu, L. Jiang, H. Wang, et al., Small 15 (2019) 1901008.
[167] Q. Zhang, H. Gu, X. Wang, et al., Appl. Catal. B 298 (2021) 120632.
[168] Z. Jin, Y. Liu, X. Hao, J. Colloid Interface Sci. 567 (2020) 357–368.
[169] X. Shi, L. Mao, P. Yang, et al., Appl. Catal. B 265 (2020) 118616.
[170] Q. Wang, G. Zhang, W. Xing, et al., Angew. Chem. 135 (2023) e202307930.
[171] S. Shen, L. Zhao, L. Guo, Mater. Res. Bull. 44 (2009) 100–105.
[172] S. Zhang, X. Liu, C. Liu, et al., ACS Nano 12 (2018) 751–758.
[173] Y. Xiao, Z. Peng, W. Zhang, et al., Appl. Surf. Sci. 494 (2019) 519–531.
[174] Y. Lei, C. Yang, J. Hou, et al., Appl. Catal. B 216 (2017) 59–69.
[175] T.F. Yeh, C.Y. Teng, S.J. Chen, H. Teng, Adv. Mater. 26 (2014) 3297–3303.
[176] X. Meng, C. Zhang, C. Dong, et al., Chem. Eng. J. 389 (2020) 124432.
[177] M.C. Biswas, M.T. Islam, P.K. Nandy, M.M. Hossain, ACS Mater. Lett. 3 (2021) 889–911.
[178] M. Sandroni, R. Gueret, K. Wegner, et al., Energy Environ. Sci. 11 (2018) 1752–1761.
[179] T. Su, C. Men, L. Chen, et al., Adv. Sci. 9 (2022) 2103715.
[180] S. Zhang, Z. Zhang, Y. Si, et al., ACS Nano 15 (2021) 15238–15248.
[181] Y. Liu, Q. Zhu, M. Tayyab, et al., Solar RRL 5 (2021) 2100536.
[182] Y.X. Tan, Z.M. Chai, B.H. Wang, et al., ACS Catal. 11 (2021) 2492–2503.
[183] A. Kumar, V. Krishnan, Adv. Funct. Mater. 31 (2021) 2009807.
[184] L. Hao, H. Huang, Y. Zhang, T. Ma, Adv. Funct. Mater. 31 (2021) 2100919.
[185] X. Deng, P. Chen, X. Wang, et al., Sci. China Mater. 66 (2023) 2299–2307.
[186] Z. Li, X. Meng, Z. Zhang, J. Photochem. Photobiol. C 35 (2018) 39–55.
[187] Z. Liang, Y. Xue, Y. Guo, et al., Chem. Eng. J. 396 (2020) 125344.
[188] J. Qiu, W. Zheng, R. Yuan, et al., Appl. Catal. B 264 (2020) 118514.
[189] W. Zhou, Z. Yin, Y. Du, et al., Small 9 (2013) 140–147.
[190] E. Parzinger, B. Miller, B. Blaschke, et al., ACS Nano 9 (2015) 11302–11309.
[191] Q. Xu, L. Zhang, B. Cheng, et al., Chem 6 (2020) 1543–1559.
[192] R. Jiang, L. Mao, Y. Zhao, et al., Sci. China Mater. 66 (2023) 139–149.
[193] N. Li, X. Gao, J. Su, et al., Chin. J. Catal. 47 (2023) 161–170.
[194] M. Cai, Y. Liu, K. Dong, et al., Chin. J. Catal. 52 (2023) 239–251.
[195] X. Wu, G. Chen, J. Wang, et al., Acta Phys. Chim. Sin. 39 (2023) 2212016.
[196] T. Li, N. Tsubaki, Z. Jin, J. Mater. Sci. Technol. 169 (2024) 82–104.
[197] G. Ding, Z. Wang, J. Zhang, et al., EcoEnergy 2 (2024) 22–44.
[198] X. Shi, C. Dai, X. Wang, et al., Nat. Commun. 13 (2022) 1287.
[199] H. Mai, T.C. Le, D. Chen, et al., Chem. Rev. 122 (2022) 13478–13515.
[200] M.F. Calegari Andrade, H.Y. Ko, L. Zhang, et al., Chem. Sci. 11 (2020) 2335–2341.
[201] Y. Li, L. Yang, H. He, et al., Nat. Commun. 13 (2022) 1355.
[202] Z. Jin, X. Wang, Mater. Today Energy 30 (2022) 101164.
[203] G. Liu, G. Zhao, W. Zhou, et al., Adv. Funct. Mater. 26 (2016) 6822–6829.
[204] B. Mei, K. Han, G. Mul, ACS Catal. 8 (2018) 9154–9164.
[205] W. Hu, L. Xie, C. Gu, et al., Coord. Chem. Rev. 506 (2024) 215715.
[206] P. Wang, T. Wang, R. Qin, et al., Adv. Energy Mater. 12 (2022) 2103359.
[207] H. Sun, Y. Ma, Q. Zhang, C. Su, Trans. Tianjin Univ. 27 (2021) 313–330.
[208] Y. Zhang, L. Ran, Z. Li, et al., Trans. Tianjin Univ. 27 (2021) 348–357.
[209] M. Li, H. Li, H. Fan, et al., Nat. Commun. 15 (2024) 6154.
[210] W. Cai, Z. Qian, C. Hu, et al., Chem. Eng. J. 479 (2024) 147718.
[211] M. Li, L. Shen, M.Q. Yang, Trans. Tianjin Univ. 28 (2022) 506–532.
[212] F. Yu, Q. Deng, H. Li, et al., Appl. Catal. B 323 (2023) 122180.
[213] X. Lin, S.F. Ng, W.J. Ong, Coord. Chem. Rev. 471 (2022) 214743.
[214] M. Ahmad, J. Chen, J. Liu, et al., Carbon Energy 6 (2024) e382.
[215] T. Liu, W. Zhu, N. Wang, et al., Adv. Sci. 10 (2023) 2302503.
[216] X. Liu, X. Yang, X. Ding, et al., Chin. Chem. Lett. 34 (2023) 108148.
[217] P.M. Ismail, S. Ali, S. Ali, et al., Adv. Mater. 35 (2023) 2303047.
[218] X. Chen, W.G. Pan, R.T. Guo, et al., J. Mater. Chem. A 10 (2022) 7604–7625.
[219] J. Ran, W. Guo, H. Wang, et al., Adv. Mater. 30 (2018) 1800128.
[220] W. Zhang, J. Hou, M. Bai, et al., Chin. Chem. Lett. 34 (2023) 108270.
[221] W. Wang, X. Wang, M. Gao, et al., Coord. Chem. Rev. 506 (2024) 215694.
[222] Y.N. Gong, W. Zhong, Y. Li, et al., J. Am. Chem. Soc. 142 (2020) 16723–16731.
[223] K. Sun, Y. Huang, Q. Wang, et al., J. Am. Chem. Soc. 146 (2024) 3241–3249.